Dissertation zur Erlangung des Doktorgrades der
Fakultät für Chemie und Pharmazie
der Ludwig-Maximilians-Universität München

Micelle Templated Photochemistry, a New Approach to Fabricate Functional Photothermal Gold Nanoarrays

Franziska Kundrat
aus
Ludwigsfelde

2017

Erklärung

Diese Dissertation wurde im Sinne von § 7 der Promotionsordnung vom 28. November 2011 von Herrn Prof. Dr. Reinhard Fässler betreut.

Eidesstattliche Versicherung

Diese Dissertation wurde eigenständig und ohne unerlaubte Hilfe erarbeitet.

München, ...

Franziska Kundrat

Dissertation eingereicht am 31. Mai 2016.

1. Gutachter: Prof. Dr. Reinhard Fässler

2. Gutachter: Prof. Dr. Dieter Braun

Mündliche Prüfung am 20. Oktober 2016.

Für meine Familie und alle, die mich lieben und unterstützt haben.

List of manuscripts

Die vorliegende Arbeit wurde in der Zeit von Oktober 2012 bis Mai 2016 in der Arbeitsgruppe von Herrn Prof. Dr. Fässler in der Abteilung für Molekulare Medizin am Max-Planck-Institut für Biochemie in Martinsried angefertigt.

Im Verlauf dieser Arbeit wurden folgende Veröffentlichungen publiziert:

1. **Kundrat F**, Baffou G, Polleux J. Shaping and patterning gold nanoparticles *via* micelle templated photochemistry. *Nanoscale*, 2015, 7, 15814-15821.

2. Robert H, **Kundrat F**, Bermúdez-Ureña E, Rigneault H, Monneret S, Quidant R, Polleux J, Baffou G. Light-Assisted Solvothermal Chemistry Using Plasmonic Nanoparticles. *ACS Omega*, 2016, 1, 2–8.

Table of contents

Summary

Individual nanoparticles as well as assembled nanostructures play a crucial role in the development of new materials. The reason for this is that nanomaterials, with a size ranging from 1 to 100 nm, display significantly different chemical and physical properties in comparison to their bulk (or microscopic) counterpart, including altered optical, magnetic, or electric properties. Especially, gold nanoparticles proved to be very attractive platforms in a broad range of applications from optics to biology because of their inertness, well-established surface chemistry and unique optical properties. Gold nanoparticles feature enhanced light absorption when excited at their plasmonic resonance wavelength, which can be tuned from visible to near infrared light by varying size, shape or interparticle distance. Moreover, nonradiative absorption of gold nanoparticles can rapidly be converted into heat - the photothermal effect - turning them into ideal nano-sources of heat. Although plasmonic applications focused for a long time on the use of the optical properties of gold nanoparticles, light-induced heat has gained more and more attention over the past years. It allows the investigation of thermal events down to the nanoscale remotely controlled through laser irradiation. Hitherto, photothermal applications commonly utilize gold nanoparticles dispersed in various chemical environments, while the use of nanoparticle assemblies on planar substrates would allow the design of functional interfaces. Such substrates would offer a better-defined photothermal profile with potential applications in the fields of nanochemistry and biomolecular manipulation. However, the fabrication of nanoparticle-based surfaces with tuneable optical properties still rely on complex and not scalable procedures, which constitute a major limitation to prepare uniform and robust plasmonic substrates. Therefore, new strategies need to be established to simplify multi-step procedures and simultaneously control the growth, the shape and the arrangement of gold nanoparticles into functional plasmonic interfaces.

In the first part of this thesis, homogeneous and micropatterned arrays of gold nanoparticles with different morphologies were generated with a new synthetic technique, called micelle templated photochemistry **(manuscript I)**. By irradiating

surfaces made of block copolymer micellar monolayers with ultraviolet light, it is possible to synthesize gold nanoparticles without requiring any commonly used reagents, such as photosensitizers or photoresists. In this method, micelles play the dual role of nanocarriers and reactive templates in order to simultaneously synthesize and organize gold nanoparticles with a high spatial resolution. This novel technique enables the growth, the arrangement and the shaping of gold nanoparticles with tuneable plasmonic resonance wavelengths on glass substrates. Explicitly, it leads to the formation of particle arrays over arbitrarily large areas decorated with either gold deformed nanoparticles ("potatoids") or nanorings featuring enhanced photothermal properties and high heat-sustainability. Moreover, control over particle distribution is possible at the microscale level in combination with photolithographic techniques. Micropatterning structures enables surface labelling necessary for serial experiments and correlative microscopy. This makes them ideal platforms for fine-tuned heat-manipulation of chemical and biological reactions.

In the second part of this work, a new application based on the use of plasmonic substrates was introduced with substantial implications for solvothermal synthesis **(manuscript II)**. Solvothermal synthesis constitutes a well-established chemical method that involves the use of a solvent heated above its boiling point under moderate or high pressure to synthesize inorganic nanomaterials. Experimentally, this approach requires the use of a pressure sealed chamber (autoclave) to avoid solvent evaporation and sustain high pressure. Using illuminated gold nanoparticles as nanosources of heat allows performing solvothermal chemistry at ambient pressure and in an open reaction medium. This method benefits from the possibility for chemical exchange and monitoring during the reaction. The concept was successfully demonstrated by the synthesis of $In(OH)_3$ nanocrystals at the micrometric scale using optical and thermal microscopy means. The underlying mechanism involves plasmon-assisted superheating of water above its boiling point and displays faster reaction times by decreasing the heated/illuminated region. Due to much faster kinetics and higher spatiotemporal resolution than standard synthetic approaches, this plasmon-assisted method is highly attractive for fundamental

research in solvothermal synthesis and could lead to novel applications in the fields of nanomaterials deposition and patterning.

Abbreviations

BCML	block copolymer micellar lithography
CVD	chemical vapour deposition
CW	continuous wave
EISA	evaporation induced self-assembly
LED	light-emitting diodes
LUMO	lowest unoccupied molecular orbital
MB	microbubble
NIR	near infrared
OMA	optomechanical actuator
PA	photoacoustic
PACS	plasmon-assisted chemical synthesis
PACVD	plasmon-assisted chemical vapour deposition
PCR	polymerase chain reaction
PT	photothermal
SPR	surface plasmon resonance
2D	two-dimensional
3D	three-dimensional

1. Introduction

1.1. From the synthesis and the shaping of nanoparticles to their 2D assembly for tuning the optical properties of nanostructured surfaces

In 1959 Richard Feynman envisioned the manipulation of individual atoms as a novel chemical strategy to build nanomaterials and announced in his lecture "There is plenty of room at the bottom" [1]. Since then, this concept significantly moved forward the emergence of Nanotechnology.

Nanotechnology is the engineering of functional systems at the molecular scale, which leads to the fabrication of advanced functional materials at the nanoscale. Nanomaterials are defined as objects with one of their dimensions below 100 nm [2-4]. What makes nanomaterials so interesting is the fact that their physical and chemical properties are different to the ones of their bulk counterpart and vary depending on their size. There are two major effects that are responsible for this behaviour: First, in nanocrystals the number of surface atoms constitutes a large fraction of the total; Second, quantum size effects alter the electronic properties of particles. Both effects can induce significant changes of the mechanical, optical, thermal and catalytic properties of many systems, which makes them potentially interesting for new applications in many technological fields [5,6]. Nanoparticle properties are not only sensitive to size but also to morphology and composition [7]. For this reason, the synthesis of nanoparticles with precise control over these three parameters is critical for the investigation and the use of these materials in Nanotechnology.

1.1.1. Synthesis of plasmonic nanoparticles with tuneable optical properties

The trend towards miniaturization and better performance is a major motivation for the development of novel "bottom-up" approaches to synthesize nanoparticles. Among the different categories of solid materials, noble metal nanostructures and gold nanoparticles in particular proved to be very attractive platforms for applications in optics and biology, thanks to their stability, inertness, well-established surface chemistry and unique optical properties.

Indeed, gold nanoparticles feature localized plasmon resonances that enhance light absorption and scattering. Surface plasmon resonance (SPR) results from the

collective oscillation of valence electrons stimulated by incident light absorbed at their resonant frequency, which is enhanced in nanostructures due to their high surface-to-volume ratio [8-10]. Consequently, SPR results in an absorbance band with a maximum intensity centred at a defined wavelength that can be shifted from visible to near infrared, depending on structural parameters such as size, shape, interparticle spacing, and the surrounding dielectric environment. Altogether, these parameters qualify the use of gold nanoparticles for biochemical labelling, sensing and detection [11-13].

The size of individual particles influences the intensity of the plasmon band, while particle shape affects the wavelength of maximum intensity. Therefore, different particle morphologies such as gold nanorods, nanoshells, nanostars or nanocages feature different modes of SPR (Figure 1) [9]. By manipulating the particle morphology, the plasmon band can be shifted to the infrared region of the spectra. This is obtained for gold nanorods upon the anisotropic growth of preformed spherical particles, for nanocages through the facile control of the wall thickness and void size, and for nanoshells by adjusting shell thickness-to-core radius ratio [14-16]. In fact, the assessment of NIR-absorbing nanoparticles is essential in biological applications for which light penetration through tissues is required [17,18]. Even though light is blocked in the visible range by the absorption of haemoglobin and water at higher wavelengths, there exist two biological windows with optimal tissue transmission located at 650-950 nm and 1000-1350 nm, in which optimal transmission is achieved [19].

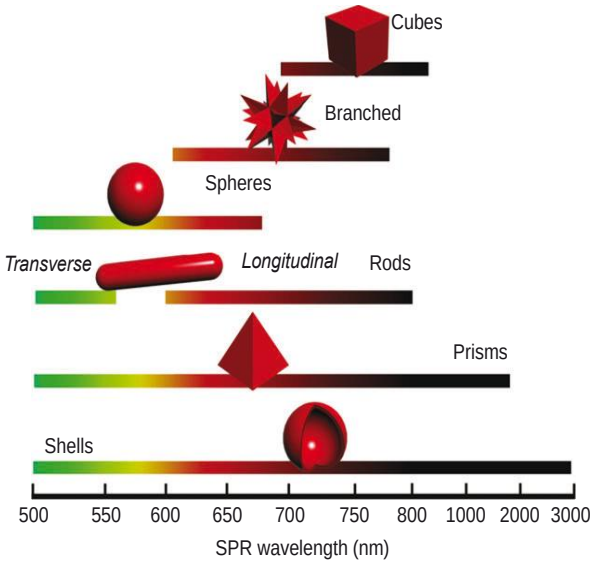

Figure 1. Scheme illustrating different nanoparticle shapes and their corresponding tuneable absorption ranges. Cubes and branched particles exhibit absorption in the near infrared region while the absorption of other shapes can be tailored over a broad range of the spectra [9].

Accordingly, many strategies to synthesize various gold nanostructures have been developed over the last twenty years in order to accurately tailor their optical properties. The Turkevic method is one of the most standard approaches to synthesize colloidal gold upon reducing a gold salt with a reducing agent such as sodium citrate [20,21]. Later, the addition of thiolated capping ligands allowed enhancing their stability to avoid particle aggregation in solution. This approach leads to the formation of monodisperse spherical nanoparticles with a particle diameter of about 12 nm [22]. However, particle monodispersity is difficult to control with this method when larger particles are produced [23]. In order to improve the synthetic process, several groups modified this approach by post-growing preformed gold nano-seeds [24], by using ultrasound irradiation [25] or upon adding block copolymers [26].

In the case of anisotropic nanostructures, similar synthetic strategies have been developed to form gold nanorods *via* template-directed, electrochemical or photochemical reduction methods [8]. Gold nanoshells are usually prepared by directly depositing gold onto colloidal silica spheres produced by the Stöber method [27]. Gold nanocages are synthesized by using silver nanocubes as a template for a galvanic replacement reaction in solution [28].

Although dispersions of gold nanoparticles of various morphologies were applied in many novel applications, the assembly of nanoparticles has also attracted a lot of attention as not only size and shape but also the interparticle distance and possibly their orientation to each other influence the absorption properties (Figure 2) [29-31]. Interparticle plasmonic coupling occurs when nanoparticles are brought in close proximity to one another. As the distance between the nanoparticles decreases, near-field coupling begins to dominate, leading to a strong enhancement of the localized electric field within the interparticle spacing resulting in a red shift of the SPR frequency [32,33]. Therefore, precise control over interparticle distance and orientation constitute an important parameter to tailor nanoparticle optical properties.

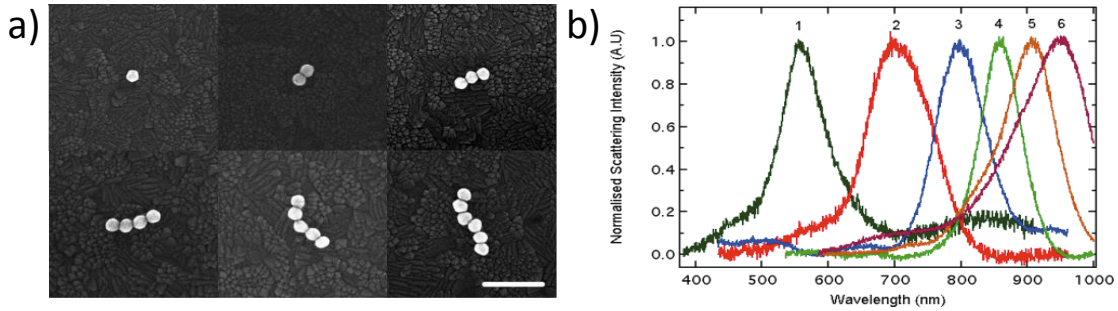

Figure 2. Effect of plasmon coupling of gold nanoparticles in close proximity. a) Surface plasmon resonances in gold nanosphere chains from monomer to hexamer and **b)** corresponding absorption spectra. Scale bar = 250 nm [29].

1.1.2. Engineering functional plasmonic substrates through the deposition of nanoparticles

In addition to their synthesis, the assembly of dispersed nanoparticles into two-dimensional (2D) and three-dimensional (3D) structures is commonly used for many applications, like for instance in colorimetric detection of polynucleotides *via* polymeric networks of nanoparticles [34] and plasmonic-rulers [35]. Importantly, the ability to tune the spatial positioning with nanometre precision enables the fabrication of materials with well-defined local-field enhancements, necessary for fundamental optical studies and the development of functional substrates/devices. The assembly of nanoparticles into 2D and 3D lattices has been studied for nearly 20 years. However, fabrication of arbitrary large nanostructured substrates composed

of nanoparticle building blocks remains challenging [33]. One possible strategy for the deposition of nanostructures in 2D involves the combination of physical means with lithographic methods, in which a geometric pattern of a resist layer is transferred onto a flat substrate in order to locally control the etching or deposition of a material of interest [36-40]. Although lithographic techniques are powerful tools to explore a wide range of nanomaterials geometries and applications with the advantages of excellent control over size, shape and interparticle spacing, a resolution below 10 nm is not readily obtainable. Moreover, the fabrication of small or crystalline structures is difficult to accomplish and their use restricted to materials that can be derived from metal films [13]. Therefore, other strategies to deposit nanoparticles have been developed [41].

The deposition and assembly of dispersed nanostructures onto surfaces constitutes a simple alternative to fabricate plasmonic substrates. One possibility here relies on the self-assembly of colloids onto surfaces by controlled evaporation, spin-coating, electrophoretic deposition, electrostatic deposition, convective assembly or liquid interface-mediated methods [42,43]. However, these approaches enable the fabrication of nanoparticle-based substrates, which are not sufficiently robust to resist certain chemical conditions or mechanical forces. To overcome this limitation, the covalent attachment of gold colloids onto aminated or thiolated surfaces is another route resulting in 2D extended arrays of gold nanoparticles, but without precise control over positioning [41,44]. DNA-mediated self-assembly methods, like DNA-origami, enable the fabrication of highly regular and uniform superstructures. DNA nanostructures are reliable templates for bottom-up assembly and fabrication of nanomaterials [45]. However, this approach suffers from the high cost of DNA and the high error rate of self-assembly [46].

Another strategy to accomplish precise positioning of metallic nanostructures on surfaces involves the use of structured polymers as a template to guide nanoparticle assembly. Block copolymer micellar lithography (BCML), is a versatile method to produce patterned gold nanoparticles arrays with sub-30 nm resolution over arbitrarily large areas [47-50]. Amphiphilic diblock copolymers can undergo microphase segregation in solvents selective for one of the two blocks, resulting in the formation

of supramolecular structures depending on temperature, molecular concentration and single molecule morphology (Figure 3) [51].

Figure 3. Morphologies of diblock copolymers. From left to right structures include spheres, hexagonal cylinders, cubic bicontinous gryoid and lamellar morphologies [52].

In order to transfer and organize these structures from solution to substrates, evaporation-induced self-assembly (EISA) is performed by dip- or spin-coating. EISA enables the deposition of a single layer of micelles on the substrate with a quasi-hexagonal order driven by capillary forces, repulsive electrostatic and steric interactions (Figure 4) [53]. Hereby, the spacing between the micelles is controlled by the molecular weight of the polymer, the concentration of the polymer solution and the dipping speed [54].

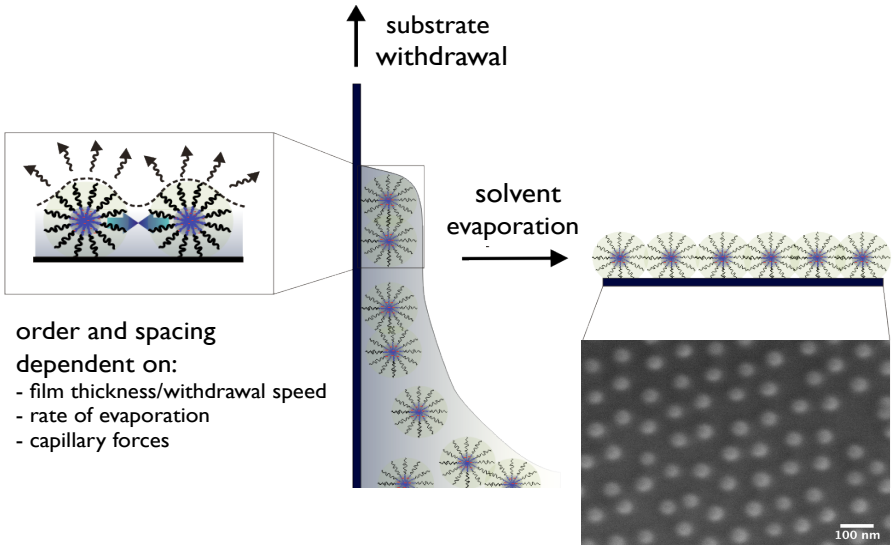

Figure 4. Schematic representation of evaporation-induced self-assembly (EISA) during dip-coating. A glass slide is dipped into a micellar solution and withdrawn at a defined speed leading to the formation of an ordered micellar monolayer, adapted from [55].

Many approaches have been successfully combined with BCML to generate plasmonic nanoparticle-based substrates including thermal evaporation [56], reactive ion etching [57], atomic layer deposition [58], galvanic displacement [59-61] or electrochemical plating [62,63]. The extended and ordered domains of self-assembled block copolymer molecules can serve as a template to selectively control the deposition of molecular precursors or inorganic nanoparticles. On the one hand,

nanoparticle arrays are obtained with BCML by the incorporation of metallic molecular precursors in the core of polymer micelles serving as nanocarriers. Metal precursors are then reduced and organic compounds removed, leading to the formation of arrays of ordered nanoparticles whose size can be further controlled *via* hydroxylamine- or ethanolamine-assisted post growth [64,65]. On the other hand, preformed nanoparticles can simply be immobilized through electrostatic interactions on preformed micellar monolayers as underlying templates [66-69].

In order to improve the adjustment of particle number and distribution on the surface independent of interparticle spacing, BCML has been combined with conventional top-down technologies. The preparation of such micropatterned surfaces is of substantial importance in the field of bioengineering for the development of microchip-based bioassays, the co-culture of cells and for tissue engineering applications [70]. The ability to guide the location of cell growth or confine their shape based on the spatial distribution of micropatterned substrates enables cell screening and the study of cell behaviour at the single-cell level or cell colonies in defined geometries without mechanical interference [71]. Micropatterned surfaces are obtained by lithographic techniques such as electron beam-lithography [72,73], microcontact printing [74] or resist-assisted particle removal [75] (Figure 5). Electron-beam lithography occurs to be time-consuming but permits patterning of individual particles by precise pinning of single micelles with an electron beam. The deposition of micelles using polymer stamps *via* microcontact printing allows faster sample processing, but patterning at the submicron range cannot be realized. In an effort to accelerate the micropatterning process, photo- and electron-beam-lithography was applied to a nanoparticle array covered by a photoresist, which resulted in significantly improved turnover rates [54].

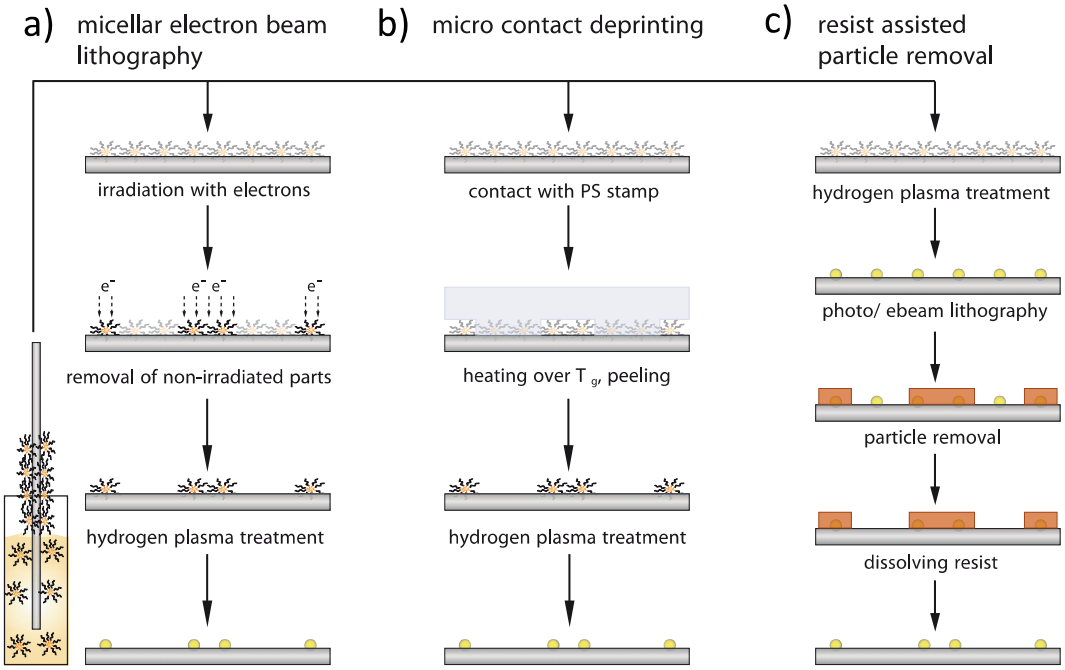

Figure 5. Illustration of micropatterning-methods compatible with BCML. **a)** Micellar electron beam lithography: patterns are written into a micellar monolayer with an electron beam. Removal of nonirradiated micelles followed by plasma treatment leads to the respective micronanostructured gold particles. **b)** Microcontact deprinting: a topographically micropatterned PS stamp is placed on a micellar monolayer and micelles in contact with the protrusions of the stamp removed by peeling off the stamp at temperatures above the glass transition temperature T. Subsequent plasma treating generates the desired nanoparticle pattern. **c)** Resist-assisted particle removal: extended arrays of gold nanoparticles are covered under a resist, followed by its photo- or electron beam-lithographic structuring. After removal of the particles in unprotected regions, the resist is dissolved and uncovers the micronanostructure [54].

Nevertheless, every method has its own pitfalls as they either require elaborate, time-consuming and multi-step processes or do not allow uniform assembly over large areas [15,76-78].

Recently, the use of deep UV-lithography enabled faster processing with benchtop facilities: Zhu *et al.* prepared micropatterned gold nanoparticle arrays by illuminating gold-loaded micellar monolayers with deep UV through a quartz photomask, minimizing the number of processing steps (Figure 6) [65].

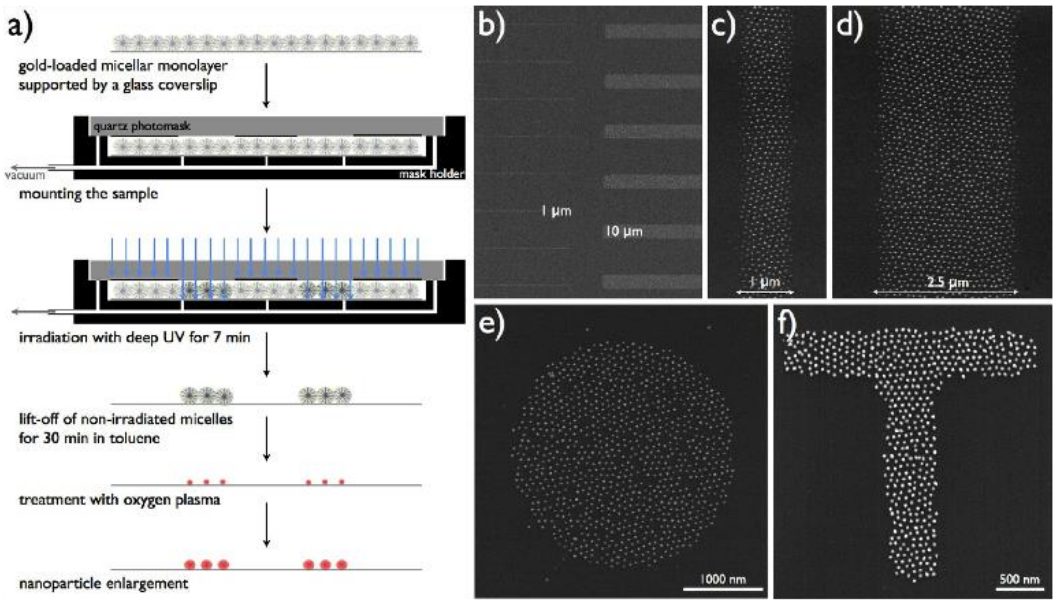

Figure 6. Generation of micropatternd gold nanoparticle arrays by using deep ultraviolet lithography and micellar nanolithography. a) Schematic diagram illustrating the successive steps necessary to fabricate micropatterned gold nanoparticles. **b-f)** SEM images of micropatterned gold nanoarrays of various shapes and dimensions [65].

However, tuning the morphology of gold particles obtained by BCML is restricted to spherical nanoparticles that only absorb at around 520 nm and micrometre-long nanowires that display a broad longitudinal plasmon resonance in the infrared due to their polydispersity in length [79,80]. To overcome this limitation, several methods were established by using spherical particles as seeds to further manipulate their shape and obtain anisotropic morphology [81-83]. However, these approaches lead to inhomogeneous arrays comprised of different particle morphologies, sizes and orientation (Figure 7).

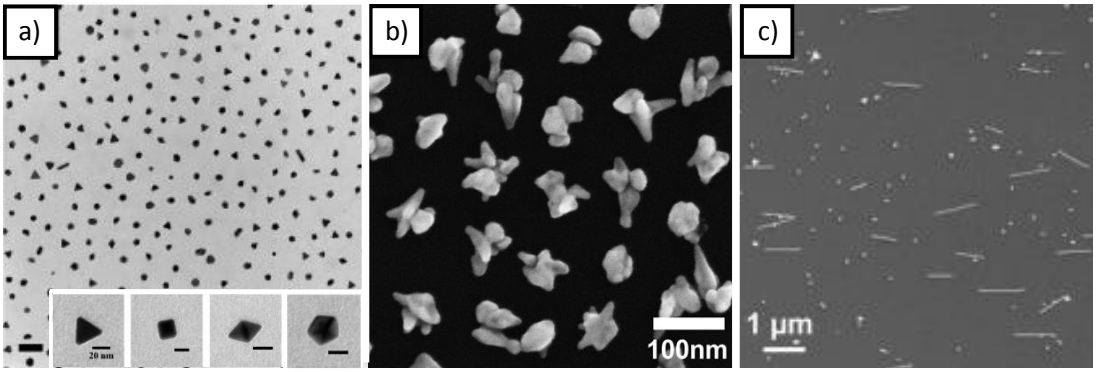

Figure 7. Tuning optical properties of gold nanoparticle-based substrates by manipulating their morphology. Immobilized gold nanoparticles act as seeds to mediate the growth of **a)** triangle, square, diamond, pentagon, and hexagon (scale bars: 100 nm and 20 nm, respectively) [81], **b)** urchin-shaped particles [82] and **c)** rod-shapes particles [83].

In conclusion, the combination of different methods is a promising strategy to prepare nanostructures with a pre-determined geometry at multiple length scales, from the microscale down to the nanoscale. However, the shaping, assembly and patterning of gold nanoparticles into functional plasmonic substrates in a facile, cost-effective and scalable manner is still challenging. The engineering of functionalized nanostructured surfaces for the development of lab-on-a-chip devices will tremendously facilitate fundamental optical studies [31], applications in nanocatalysis [84], biosensing [13,85] and photothermy [16,86].

1.2. The photothermal effect and its applications in nanochemistry and biomolecular manipulation

For a long time, plasmonic applications focused mainly on the use of the optical properties of gold nanoparticles [87-89]. However, light-induced heat has gained more and more attention over the past years. Nonradiative absorption of gold nanoparticles can rapidly be converted into heat, the so-called photothermal effect, turning them into ideal nano-sources of heat, which allows the investigation of thermal events down to the nanoscale remotely controlled through laser irradiation. Under continuous wave (CW) laser illumination, the achieved temperature increase depends on parameters such as the absorption cross-section and shape of nanoparticles, the thermal conductivity of the surrounding medium, as well as the wavelength and irradiance of the incoming light. Pulsed illumination on the other hand can lead to structural remodelling of the nanoparticle, extreme thermodynamic conditions, improved spatiotemporal heat confinement, and pressure variations leading to acoustic wave and bubble formation [86]. Conversion into heat occurs at the rate of approximately 1 ps by fast electron-phonon and phonon-phonon processes (Figure 8). Upon irradiation, the gas of free electrons of the nanoparticle absorbs part of the incident pulse energy. In this process, the temperature of the electronic gas increases while the temperature of the lattice (phonons) remains unchanged. Subsequently, this hot electronic gas cools down through internal electron-phonon relaxation. Finally, the energy of phonons is

dissipated into the surrounding medium and leads to a cooling of the nanoparticle and a heating of the surrounding medium [13]. The spatial extension of the temperature distribution in the surroundings varies with 1/r under CW illumination, while pulsed illumination further confines the temperature increase at the vicinity of the nanoparticle [86].

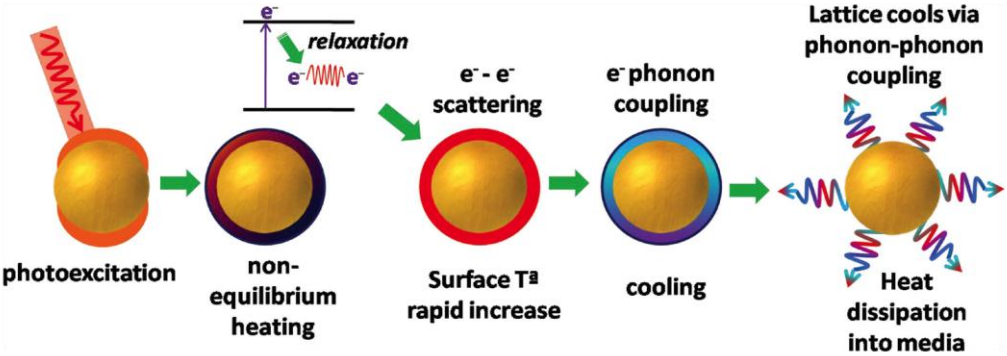

Figure 8. Process of photoexcitation transforming light into heat. Absorption of a photon stimulates a free electron from the gold nanoparticle to reach a higher energy level. This electron loses energy through electron-electron scattering followed by electron-phonon coupling leading to cooling of the particle by release of heat into the surrounding media [90].

Recently, Baffou *et al.* observed that gold substrates are also capable to induce superheating under CW illumination, a phenomenon where a liquid is heated above its boiling point. Superheating only occurs when no nucleation centres like cavities, impurities or scratches are present on the surface that is heated. Under these conditions, microbubbles (MB) have been observed under continuous illumination on planar substrates of spherical gold nanoparticles in water at temperatures far above the boiling point of water (between 220 - 240 °C). Notably, in contrast to bubbles generated under pulsed illumination these MB consist of air instead of water steam coming from the air molecules dissolved in the surrounding water [91]. This light-induced superheating could create similar conditions as in autoclaves opening new opportunities such as laser-assisted solvothermy. (Manuscript II)

1.2.1. Light-assisted chemistry using plasmonic nanoparticles

Plasmon-induced nanochemistry is a growing research area benefiting from the light harvesting properties of plasmonic nanoparticles that can provide photo-induced electrons or heat to initiate chemical reactions [92]. Nanostructures offer high spatial and temporal resolution for chemical reactions down to the nanoscale. On the one

hand, chemical reactions are promoted by the enhanced optical near field [93-95] of nanoparticles at the vicinity of the illuminated particles. On the other hand, heat generation favours local chemical synthesis according to the Arrhenius law. Hot electron/hole injection [96-98] has also been proposed to induce localized redox reactions.

Plasmonic nanostructures can catalyse chemical reactions in different ways, either directly on its surface or in hybrid materials by enhancing catalytic activity of semiconductors (Figure 9). The latter one is based on an energy transfer process, where the plasmonic nanoparticle acts as a donor absorbing light energy. This energy in form of electrons is then transferred to the semiconductor acting as acceptor (plasmonic sensitization). On the contrary, pure-metal plasmonic catalysis is typically attributed to the local heating of the plasmonic structure upon excitation or the electron injection to the lowest unoccupied molecular orbital (LUMO) of the reactant molecule [92,99].

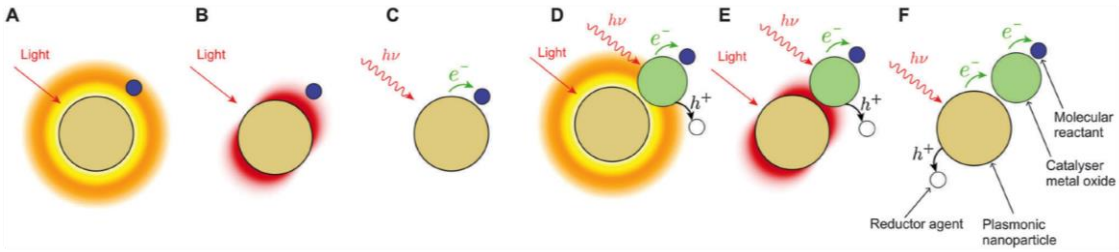

Figure 9. Mechanisms underlying reaction catalysis utilizing plasmonic nanostructures. In direct plasmonic catalysis, the nanoparticle absorbs and transforms light energy and generates heat (A), an increased optical near-field (B) or electrons (C) to a nearby reactant. In metal-semiconductor systems the generation of electron-holes are enhanced by the photo-induced heat (D) or the strong optical near-field (E). Another possible mechanism is the hot electron injection from the nanoparticle to the adjacent photocatalyst (F) [92].

In the past years, nanochemistry has been successfully applied in many chemical reactions, such as the synthesis of metal oxides on glass substrates with high spatial control of material deposition *via* plasmon-assisted chemical vapour deposition (PACVD), also called plasmon-resonant CVD (Figure 10a) [100-103]. Furthermore, plasmon-assisted catalysis in gas phase [104,105] or in liquids (Figure 10b) [106] has been shown as well as the thermal decomposition of peroxides [107]. Moreover, it has been demonstrated that gold nanoparticles facilitate various other chemical reaction, including photodecomposition of organic pollutants, solar water splitting, and organic synthesis [99].

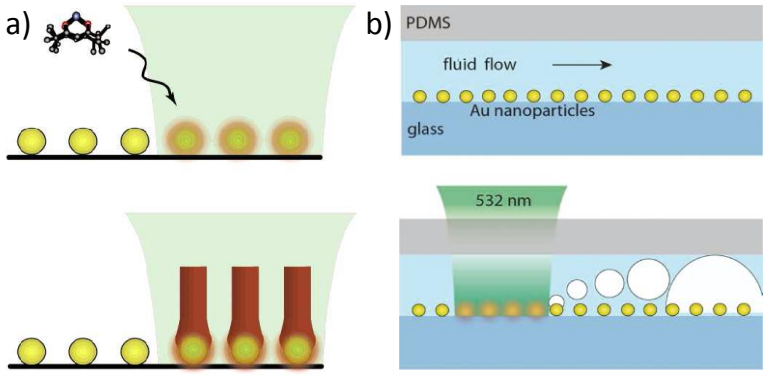

Figure 10. Light-assisted chemistry using plasmonic nanoparticles. Schematic illustration of **a)** metal oxide deposition on glass substrates *via* plasmon-assisted chemical vapour deposition [102] and **b)** Plasmon-assisted catalysis in gas phase [106].

Solvothermal chemical synthesis can also benefit from plasmonic substrates. In solvothermal chemistry, reactions are enhanced due to thermal phenomena such as high reactivity of reactants and the formation of a metastable solvent that increases solubility of the reactants [108]. As mentioned above, it has been recently shown, that water superheating can be achieved at ambient pressure by heating plasmonic nanoparticles immobilized on a glass substrate by using a continuous wave laser illumination [91]. This observation could tremendously facilitate solvothermal chemical synthesis that is normally accomplished in a sealed chamber (autoclave), in which the temperature increase concomitantly creates a pressure increase that maintains the solvent in a liquid state. The use of an autoclave also prevents from any chemical exchange and monitoring during the reaction. By using plasmonic substrates as heat sources, many of these limitations could be overcome while simultaneously enabling the observation of product formation using optical means. Plasmon-assisted chemical synthesis (PACS) will additionally allow much faster heating/cooling dynamics, as the temperature rises or vanishes as soon as the laser illumination is turned on or off due to the weak inertia related to the small volume of the system. Therefore, PACS could not only move forward fundamental research in solvothermal synthesis, but could also yield to applications in local patterning of nanostructures. (Manuscript II)

1.2.2. Plasmonic substrates for applications in diagnostics and cellular manipulation

In addition to its use in nanochemistry, spatiotemporal control of light-induced heat with the help of gold nanoparticles proved to be a versatile tool in many biological applications. For example, surface-engineered gold nanoparticles have been applied in gene/drug delivery and the photothermal treatment of cancer. Due to the highly efficient and localized light-to-heat conversion of gold nanoparticles, only minimal irradiation is required to release bioactive molecules from the particle surface or induce tumour cell death. Therefore, the illumination of plasmonic nanoparticles constitutes a minimally invasive approach with a promising potential for disease therapy [10,109,110]. The use of gold nanoparticles also rapidly emerged in the area of imaging, including photothermal (PT) and photoacoustic (PA) imaging. These techniques are based on the nonradiative conversion of absorbed laser energy into heat (PT imaging) and the accompanying formation of bubbles and acoustic waves (PA imaging) [111-113]. Interestingly, PT/PA imaging can be combined with photothermal destruction of tumors, making gold nanoparticles a multifunctional platform of choice in the treatment of cancer [114]. Plasmonic nanoparticles have also been used for the manipulation of cells down to the molecular scale by thermally activating cell surface receptors such as ion channels in neuronal cells [115]. However, less effort has been focused on the development and use of gold nanoparticle-based substrates, which would enable a more accurate spatiotemporal control of heat generation and could be utilized as functional platforms for applications ranging from biochemical analysis to the manipulation of molecules and cells.

In the context of biological analysis, photothermal substrates were shown to accelerate and miniaturize the process of DNA amplification. Researchers used photothermal heating of gold thin films to accelerate the process of the polymerase chain reaction (PCR). This new system is comprised of a disposable PCR chip using light-emitting diodes (LEDs) to induce light-to-heat conversion of the gold film (Figure 11). The authors demonstrated the successful nucleic acid amplification by ultrafast thermal cycling accomplished within 5 min. This ultrafast photonic PCR

could be generally integrated into a variety of devices as it is inexpensive, compact (no heating blocks) and equipment-free (only LED, microcontroller modules, cellphone camera) [116].

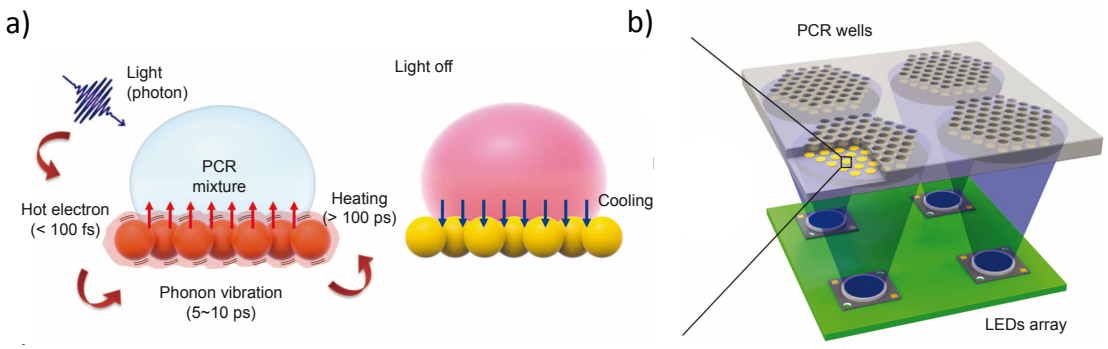

Figure 11. Scheme of PCR on plasmonic substrates. a) Schematics of the plasmonic photothermal light-to-heat conversion, subsequent heating of the surrounding PCR mixture and fast cooling after light is turned of by heat dissipation through the thin Au film. b) Set-up for multiple PCR reactions [116].

Furthermore, the ability to control the motion of micro/nano-objects in solution has become important in biological analysis. Today, optical tweezer systems are commonly used for the trapping and manipulation of cells and particles, but are limited to mesoscopic systems due to the diffraction-limited focus of a laser beam [117,118]. This led to the development of other techniques such as thermophoresis, where particle motion is induced by generating a temperature gradient (Ludwig-Soret effect) [119]. Thermophoretic trapping has been demonstrated for DNA, RNA and colloids, however trapping was only possible for large ensembles of molecules and colloids [120-125]. More recently, plasmonic substrates have been used as sources of heat in thermophoretic trapping of particles and cells [126-128]. In contrast to conventional laser-induced thermophoresis, the use of plasmonic substrates enables trapping down to the dimension of a single nano-object [129]. Moreover, plasmon-assisted trapping can be integrated with microfluidics for lab-on-a-chip applications. It has become significant in the development of future miniaturized analytical devices due to the small volumes required and the possibility to perform many sample analyses in parallel. Moreover, “plasmonic chips” are attractive, as no complex microfluidic designs are required such as pumps, valves or electrode patterning [86].

Plasmonic substrates can also be used to manipulate the extracellular environment of cells spread over nanoparticles. Over the last decade, many different approaches have been developed to substitute the standard procedure of cell harvesting *via* enzyme digestion by either using physicochemical stimuli, such as variations of pH [130], temperature [70] or electrochemical potential [131], but also photocleavable polymers [132]. Although some of these methods are sufficient to detach cells from their extracellular environment, significant cellular damages are unavoidable and substrate fabrication require significant synthetic efforts. Recently, researchers reported that laser-induced cell detachment is possible in a reversible manner with high cell viability by using gold nanoparticle-based surfaces. Although damages to the cell membrane *via* photochemical generation of reactive oxygen species (ROS) were made, Kolesnikova *et al.* showed the reversible detachment and patterning of fibroblasts in ring-like shapes on gold nanoparticles under green laser illumination of low intensity (Figure 12a) [133]. Giner-Casares *et al.* also demonstrated efficient cell detachment with high cell viability by using a dense array of branched gold nanostructures irradiated with near infrared (NIR) light (Figure 12b). The authors claimed that local heat effects confined to the proximity of the substrate directly induced cell detachment since photochemical generation of ROS is unlikely to happen under NIR illumination [134].

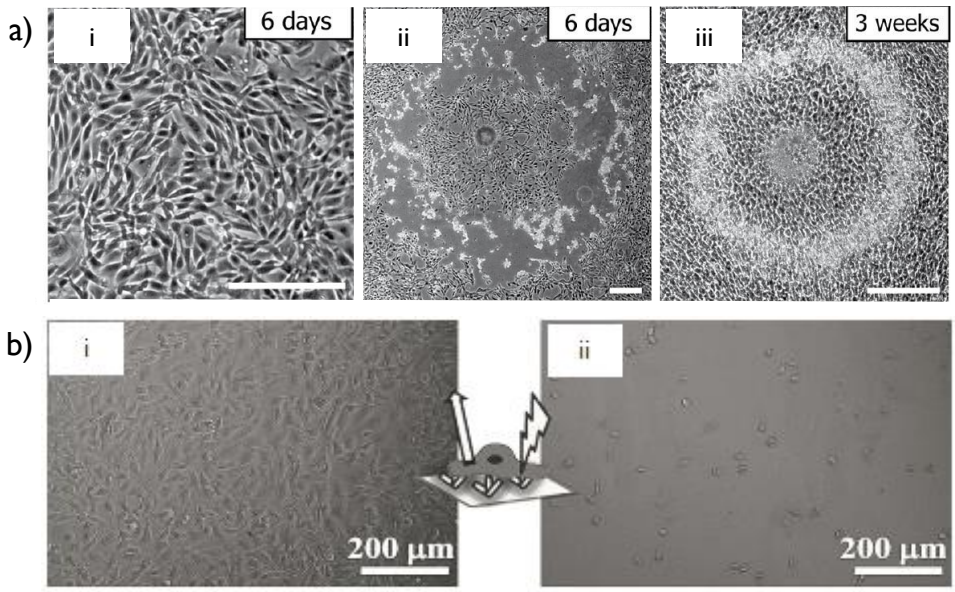

Figure 12. Plasmon assisted cell harvesting and patterning. a) Phase contrast microscopy image of fibroblast adhesion (6 days of cell culturing) (i) and ring-shaped detachment of cells from plasmonic surfaces after laser irradiation (532 nm, 750 mW, 2 min) in dependence on the cell age (6 days (ii) and 3 weeks (iii) of culture. Scale bar = 300 µm [133]. **b)** Transmitted light images of HeLa cells grown on glass or plasmonic substrates (before (i) and after (ii) irradiation with a NIR laser at 980 nm [134].

In contrast to cell detachment, it has been shown that the manipulation of cell adhesion could be achieved in a reversible manner with subcellular resolution by using photothermal substrates. Zhu *et al.* developed biofunctionalized micropatterned arrays of gold nanoparticles that confine cell migration along one direction and function as plasmonic nanostoves to create heat gradients in the vicinity of the cell. In such experimental conditions, it is possible to locally stop the formation of new adhesion sites, allowing both blocking and guiding cell migration (Figure 13). Photothermal cell manipulation is reversible and not restricted spatiotemporally, which could enable further study of the complex connections between the extracellular environment and the cell. However, this approach requires the use of a green laser to heat the nanoparticles, which is phototoxic for the cell and incompatible with fluorescent imaging techniques due to fluorophore bleaching. To overcome this, the development of near-infrared absorbing substrates would be necessary [65].

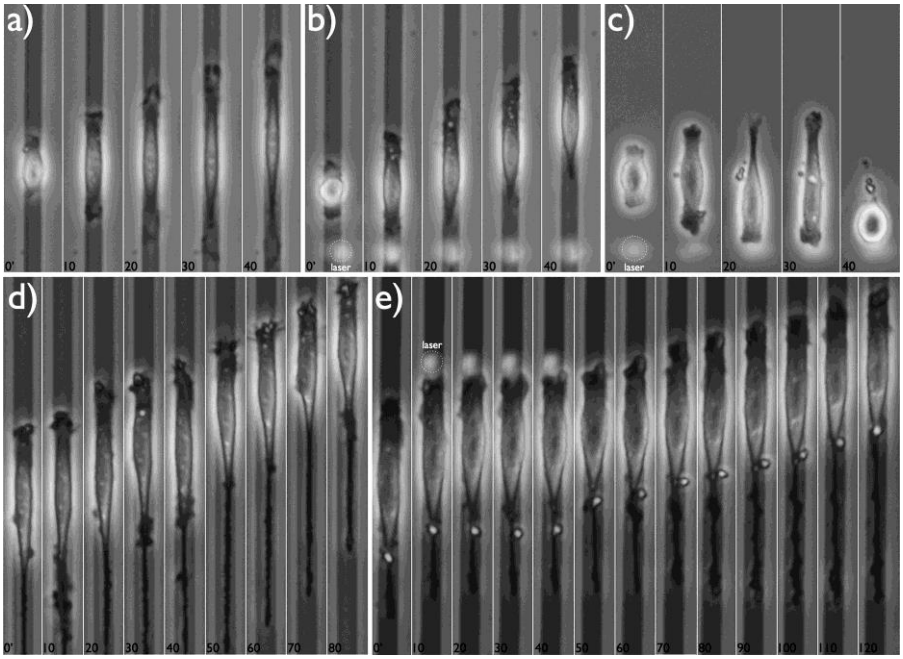

Figure 13 Heat-assisted manipulation of cell adhesion during spreading and migration. a) Cell migration upon isotropic spreading on plasmonic substrates without laser illumination. Cell migration upon isotropic spreading with laser illumination on **b)** plasmonic substrates or **c)** glass coverslips. Cell migration on plasmonic substrates **d)** without and **e)** with laser illumination. The latter condition blocks cell migration [65].

More recently, Liu *et al.* developed an optomechanical actuator (OMA) by functionalizing near-infrared absorbing substrates with a thermo-responsive polymer, which undergoes a structural transition from extended to compact during laser illumination (Figure 14). Upon conjugating bioactive ligands to the polymer, OMA can be used to locally apply mechanical forces to ligand-bound receptors, which induce cell protrusions and mediate focal adhesion formation by the optical manipulation of integrin tension. With this approach, receptor mechanics can be controlled with high spatiotemporal resolution. Moreover, the amplitude, duration, repetition and loading rate of the mechanical input can be administered through the NIR-pulse [135].

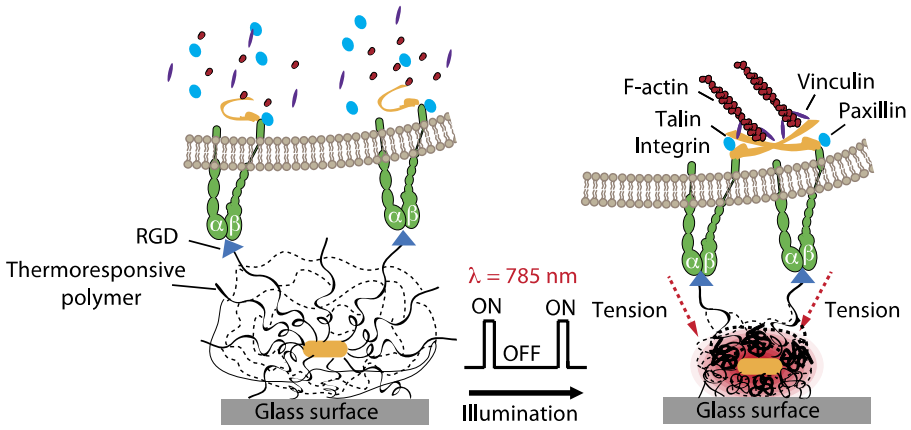

Figure 14. Schematic illustration of optomechanical actuator (OMA) nanoparticles. Depicted are the general design and proposed mechanism of OMA nanoparticles [135].

In contrast to optogenetics [136,137], the described approaches do not require genetic modifications as manipulation is performed extracellulary and can be extended to different cell surface receptors by using a large variety of available ligands. Consequently, the manipulation of cell surface receptors can be molecularly selected, enabling further dissection of signalling circuits between cells and their environment.

In summary, gold nanoparticle-based substrates display many advantages over dispersed particles, as particle aggregation does no take place. Therefore, such substrates exhibit a well-defined absorption and generate plasmonic heat in a homogeneous and reproducible manner. Moreover, as immobilized particles are not internalized into the cell, issues such as cytotoxicity and biodistribution can be circumvented and substrates reused upon plasma cleaning. Additionally, the use of particle-based substrates offers higher spatial resolution for molecular manipulation as the heated area is not only defined by the focused laser beam but also by nanoparticle distribution upon micropatterning [65,138] and the temporal profile of illumination. Upon pulsing down to the femtosecond heat can be confined to the vicinity of individual nanoparticles. Photothermal plasmonic substrates helped to improve many techniques [116,126] or enabled the development of new methods [92,134,135]. In the future, there is plenty of room to establish more applications to further dissect the biology of the cell by fluorescent microscopy, such as the investigation of thermotaxis mediated by light-induced temperature

gradients, localized heat stress on the heat shock response activation or heat-induced neuronal guidance.

2. Aim of the thesis

In the past two decades, nanotechnology has led to the development of novel valuable tools critical for the manipulation and the characterization of nano-sized objects in the fields of material science, chemistry, biology and medicine. Nanomaterials - defined as objects with one of their dimensions below 100 nm - possess physical and chemical properties that differ to the ones of their bulk counterpart. Particularly, gold nanoparticles have attracted a lot of attention due to their exceptional properties including biocompatibility and well-established surface chemistry. Gold nanoparticles also feature unique optical properties with localized plasmon resonances that enhance light absorption and scattering associated to parameters such as nanoparticle size, shape, interdistance, and surrounding dielectric environment. Accordingly, nanoparticle absorption wavelength can be shifted from the visible to the near infrared region of the light spectrum by manipulating these parameters. Furthermore, gold nanoparticles can transform absorbed light into heat, commonly referred to as the photothermal effect. This event turns particles into ideal nano-sources, which provides a unique way to control thermal-induced phenomena down to the nanoscale. Light-induced heat generated by dispersed gold nanoparticles proved to be a versatile tool not only in many biological applications, but also in nanochemistry. However, less effort has been devoted on the development and use of gold nanoparticle-based substrates, which would enable a more accurate spatiotemporal control of heat generation and could be utilized as functional platforms for applications ranging from biochemical analysis to the manipulation of molecules and cells. However, the fabrication of functional nanostructured substrates capable to perform highly adjustable heat-manipulation remains challenging, as they must fulfil many requirements including robustness and scalability.

The main aim of this thesis was to establish a simple synthetic method to control the growth, the shape and the arrangement of gold nanoparticles on flat surfaces in order to fabricate functional plasmonic substrates capable to generate heat with high spatiotemporal resolution for photothermal applications in nanochemistry and biomolecular manipulation. For the development of such a technique, many criteria

had to be fulfilled: 1) generation of near-infrared absorbing nanoparticle-based substrates to circumvent phototoxic effects on irradiated biological samples; 2) synthesis of nanoparticles in a homogenous and reproducible manner over arbitrarily large areas to enable fine-tuned heat-manipulation; 3) simplification of complex fabrication procedures and in addition their combination with lithographic techniques to control particle distribution at the microscale, facilitating surface labelling necessary for serial experiments and correlative microscopy; and 4) robustness, as many photothermal applications require substrate resistance to heat, various chemical conditions and/or mechanical forces.

Moreover, this work intended to introduce both a new application in plasmonics and a new paradigm in chemistry. It concerns solvothermal synthesis, a well-known method in chemistry that systematically involves the use of a pressure sealed chamber (autoclave) to facilitate chemical reactions occurring in metastable liquids above their boiling point. It was shown that solvothermal synthesis can be achieved at ambient pressure, in an open reaction medium using gold nanoparticles, which have the ability to safely superheat a fluid above its boiling point. This method is general and could be used to spatially control the deposition of virtually any material for which a solvothermal synthesis exists.

3. Short summaries of manuscripts

3.1. First Manuscript

Title: Shaping and patterining gold nanopartciles via micelle templated photochemistry

Shaping and positioning noble metal nanostructures are essential processes that still require laborious and sophisticated techniques to fabricate functional plasmonic interfaces. The present study reports a simple photochemical approach compatible with micellar nanolithography and photolithography that enables the growth, arrangement and shaping of gold nanoparticles with tuneable plasmonic resonances on glass substrates. Ultraviolet illumination of surfaces coated with gold-loaded micelles leads to the formation of gold nanoparticles with micro/nanometric spatial resolution without requiring any photosensitizers or photoresists. Depending on the extra-micellar chemical environment and the illumination wavelength, block copolymer micelles act as reactive and light-responsive templates, which enable to grow gold deformed nanoparticles (potatoids) and nanorings. Optical characterization reveals that arrays of individual potatoids and rings feature a localized plasmon resonance around 600 and 800 nm, respectively, enhanced photothermal properties and high temperature sustainability, making them ideal platforms for future developments in nanochemistry and biomolecular manipulation controlled by near-infrared- induced heat.

3.2. Second Manuscript

Title: Light-Assisted Solvothermal Chemistry using Plasmonic Nanoparticles

Solvothermal synthesis, denoting chemical reactions occurring in metastable liquids above their boiling point, normally requires the use of a sealed autoclave under pressure, to prevent the solvent from boiling. This work introduces an experimental approach that enables solvothermal synthesis at ambient pressure, in an open reaction medium. The approach is based on the use of gold nanoparticles deposited on a glass substrate and acting as photothermal sources. To illustrate the approach, the selected hydrothermal reaction involves the formation of indium hydroxide microcrystals favoured at 200°C in liquid water. In addition to demonstrating the principle, the benefits and the specific characteristics of such an approach are investigated, in particular the much faster reaction rate, the achievable spatial and time scales, the effect of microscale temperature gradients, the effect of the size of the heated area and the effect of thermal-induced microscale fluid convection. This technique is general and could be used to spatially control the deposition of virtually any material for which a solvothermal synthesis exists.

4. References

(1) Feynman, R. P. There's Plenty of Room at the Bottom. *Engineering and science* **1960**, 23, 22–36.

(2) Office, P. COMMISSION RECOMMENDATION of 18 October 2011 on the Definition of Nanomaterial. **2011**, 1–3.

(3) Bleeker, E. A. J.; de Jong, W. H.; Geertsma, R. E.; Groenewold, M.; Heugens, E. H. W.; Koers-Jacquemijns, M.; van de Meent, D.; Popma, J. R.; Rietveld, A. G.; Wijnhoven, S. W. P.; *et al.* Considerations on the EU Definition of a Nanomaterial: Science to Support Policy Making. *Regulatory Toxicology and Pharmacology* **2013**, *65*, 119–125.

(4) Kreyling, W. G.; Semmler-Behnke, M.; Chaudhry, Q. A Complementary Definition of Nanomaterial. *Nano Today* **2010**, *5*, 165–168.

(5) Ramesh, K. T. Nanomaterials. *Springer Science & Business Media* **2009**.

(6) Bréchignac, C.; Houdy, P.; Lahmani, M. Nanomaterials and Nanochemistry. *Springer Science & Business Media* **2008**, 1–747.

(7) El-Sayed, M. A. Small Is Different: Shape-, Size-, and Composition-Dependent Properties of Some Colloidal Semiconductor Nanocrystals. *Acc. Chem. Res.* **2004**, *37*, 326–333.

(8) Hu, M.; Chen, J.; Li, Z.-Y.; Au, L.; Hartland, G. V.; Li, X.; Marquez, M.; Xia, Y. Gold Nanostructures: Engineering Their Plasmonic Properties for Biomedical Applications. *Chem. Soc. Rev.* **2006**, *35*, 1084–1094.

(9) Chanana, M.; Liz-Marzán, L. M. Coating Matters: the Influence of Coating Materials on the Optical Properties of Gold Nanoparticles. *Nanophotonics* **2012**, *1*, 199–220.

(10) Dreaden, E. C.; Mackey, M. A.; Huang, X.; Kang, B.; El-Sayed, M. A. Beating Cancer in Multiple Ways Using Nanogold. *Chem. Soc. Rev.* **2011**, *40*, 3391.

(11) Boisselier, E.; Astruc, D. Gold Nanoparticles in Nanomedicine: Preparations, Imaging, Diagnostics, Therapies and Toxicity. *Chem. Soc. Rev.* **2009**, *38*, 1759–1782.

(12) Connor, E. E.; Mwamuka, J.; Gole, A.; Murphy, C. J.; Wyatt, M. D. Gold Nanoparticles Are Taken Up by Human Cells but Do Not Cause Acute Cytotoxicity. *Small* **2005**, *1*, 325–327.

(13) Jin, Y. Engineering Plasmonic Gold Nanostructures and Metamaterials for Biosensing and Nanomedicine. *Adv. Mater.* **2012**, *24*, 5153–5165.

(14) Huang, X.; El-Sayed, I. H.; Qian, W.; El-Sayed, M. A. Cancer Cell Imaging and Photothermal Therapy in the Near-Infrared Region by Using Gold Nanorods. *J. Am. Chem. Soc.* **2006**, *128*, 2115–2120.

(15) Vigderman, L.; Khanal, B. P.; Zubarev, E. R. Functional Gold Nanorods: Synthesis, Self-Assembly, and Sensing Applications. *Adv. Mater.* **2012**, *24*, 4811–4841.

(16) Boulais, E.; Lachaine, R.; Hatef, A.; Meunier, M. Plasmonics for Pulsed-Laser Cell Nanosurgery: Fundamentals and Applications. *Journal of Photochemistry and Photobiology C: Photochemistry Reviews* **2013**, *17*, 26–49.

(17) Okuno, T.; Kato, S.; Hatakeyama, Y.; Okajima, J.; Maruyama, S.; Sakamoto, M.; Mori, S.; Kodama, T. Photothermal Therapy of Tumors in Lymph Nodes Using Gold Nanorods and Near-Infrared Laser Light. *Journal of Controlled Release* **2013**, *172*, 879–884.

(18) Wang, Y.; Black, K. C. L.; Luehmann, H.; Li, W.; Zhang, Y.; Cai, X.; Wan, D.; Liu, S.-Y.; Li, M.; Kim, P.; *et al.* Comparison Study of Gold Nanohexapods, Nanorods, and Nanocages for Photothermal Cancer Treatment. *ACS Nano* **2013**, *7*, 2068–2077.

(19) Tsai, M.-F.; Chang, S.-H. G.; Cheng, F.-Y.; Shanmugam, V.; Cheng, Y.-S.; Su, C.-H.; Yeh, C.-S. Au Nanorod Design as Light-Absorber in the First and Second Biological Near-Infrared Windows for in VivoPhotothermal Therapy. *ACS Nano* **2013**, *7*, 5330–5342.

(20) Turkevich, J.; Stevenson, P. C.; Hillier, J. A Study of the Nucleation and Growth Processes in the Synthesis of Colloidal Gold. *Discuss. Faraday Soc.* **1951**, *11*, 55–75.

(21) Wuithschick, M.; Birnbaum, A.; Witte, S.; Sztucki, M.; Vainio, U.; Pinna, N.; Rademann, K.; Emmerling, F.; Kraehnert, R.; Polte, J. Turkevich in New Robes: Key Questions Answered for the Most Common Gold Nanoparticle Synthesis. *ACS Nano* **2015**, *9*, 7052–7071.

(22) Frens, G. Controlled Nucleation for the Regulation of the Particle Size in Monodrsperse Gold Solutions. *Nature Phys. Sci* **1973**, 241, 20–22.

(23) Brust, M.; Walker, M.; Bethell, D.; Schiffrin, D. J.; Whyman, R. Synthesis of Thiol-Derivatised Gold Nanoparticles in a Two-Phase Liquid-Liquid System. *J. Chem. Soc., Chem. Commun.* **1994**, 7, 801–802.

(24) Perrault, S. D.; Chan, W. C. W. Synthesis and Surface Modification of Highly Monodispersed, Spherical Gold Nanoparticles of 50−200 Nm. *J. Am. Chem. Soc.* **2009**, *131*, 17042–17043.

(25) Zhang, J.; Du, J.; Han, B.; Liu, Z.; Jiang, T.; Zhang, Z. Sonochemical Formation of Single-Crystalline Gold Nanobelts. *Angew. Chem.* **2006**, *118*, 1134–1137.

(26) Sakai, T.; Alexandridis, P. Mechanism of Gold Metal Ion Reduction, Nanoparticle Growth and Size Control in Aqueous Amphiphilic Block Copolymer Solutions at Ambient Conditions. *J. Phys. Chem. B* **2005**, *109*, 7766–7777.

(27) Dreaden, E. C.; Alkilany, A. M.; Huang, X.; Murphy, C. J.; El-Sayed, M. A. The Golden Age: Gold Nanoparticles for Biomedicine. *Chem. Soc. Rev.* **2012**, *41*, 2740–2779.

(28) Skrabalak, S. E.; Chen, J.; Sun, Y.; Lu, X.; Au, L.; Cobley, C. M.; Xia, Y. Gold Nanocages: Synthesis, Properties, and Applications. *Acc. Chem. Res.* **2008**, *41*, 1587–1595.

(29) Barrow, S. J.; Funston, A. M.; Gómez, D. E.; Davis, T. J.; Mulvaney, P. Surface Plasmon Resonances in Strongly Coupled Gold Nanosphere Chains From Monomer to Hexamer. *Nano Lett.* **2011**, *11*, 4180–4187.

(30) Funston, A. M.; Novo, C.; Davis, T. J.; Mulvaney, P. Plasmon Coupling of Gold Nanorods at Short Distances and in Different Geometries. *Nano Lett.* **2009**, *9*, 1651–1658.

(31) Halas, N. J.; Lal, S.; Chang, W.-S.; Link, S.; Nordlander, P. Plasmons in Strongly Coupled Metallic Nanostructures. *Chem. Rev.* **2011**, *111*, 3913–3961.

(32) Barrow, S. J.; Funston, A. M.; Wei, X.; Mulvaney, P. DNA-Directed Self-Assembly and Optical Properties of Discrete 1D, 2D and 3D Plasmonic Structures. *Nano Today* **2013**, *8*, 138–167.
(33) Barrow, S. J.; Wei, X.; Baldauf, J. S.; Funston, A. M.; Mulvaney, P. The Surface Plasmon Modes of Self-Assembled Gold Nanocrystals. *Nature Communications* **2012**, *3*, 1275.
(34) Elghanian, R.; Storhoff, J. J.; Mucic, R. C.; Letsinger, R. L.; Mirkin, C. A. Selective Colorimetric Detection of Polynucleotides Based on the Distance-Dependent Optical Properties of Gold Nanoparticles. *Science* **1997**, *277*, 1078–1081.
(35) Liu, N.; Hentschel, M.; Weiss, T.; Alivisatos, A. P.; Giessen, H. Three-Dimensional Plasmon Rulers. *Science* **2011**, *332*, 1407–1410.
(36) Boltasseva, A. Plasmonic Components Fabrication via Nanoimprint. *J. Opt. A: Pure Appl. Opt.* **2009**, *11*, 114001.
(37) Basnar, B.; Willner, I. Dip-Pen-Nanolithographic Patterning of Metallic, Semiconductor, and Metal Oxide Nanostructures on Surfaces. *Small* **2009**, *5*, 28–44.
(38) Fan, M.; Andrade, G. F. S.; Brolo, A. G. A Review on the Fabrication of Substrates for Surface Enhanced Raman Spectroscopy and Their Applications in Analytical Chemistry. *Analytica Chimica Acta* **2011**, *693*, 7–25.
(39) Matsui, S.; Ochiai, Y. Focused Ion Beam Applications to Solid State Devices. *Nanotechnology* **1996**, 247–258.
(40) Zhang, G.; Wang, D. Colloidal Lithography-the Art of Nanochemical Patterning. *Chem. Asian J.* **2009**, *4*, 236–245.
(41) Mendes, P. M.; Chen, Y.; Palmer, R. E.; Nikitin, K.; Fitzmaurice, D.; Preece, J. A. Nanostructures From Nanoparticles. *J. Phys.: Condens. Matter* **2003**, *15*, S3047–S3063.
(42) Zhang, J.; Li, Y.; Zhang, X.; Yang, B. Colloidal Self-Assembly Meets Nanofabrication: From Two-Dimensional Colloidal Crystals to Nanostructure Arrays. *Adv. Mater.* **2010**, *22*, 4249–4269.
(43) Vogel, N.; Retsch, M.; Fustin, C.-A.; del Campo, A.; Jonas, U. Advances in Colloidal Assembly: the Design of Structure and Hierarchy in Two and Three Dimensions. *Chem. Rev.* **2015**, *115*, 6265–6311.
(44) Grabar, K. C.; Allison, K. J.; Baker, B. E.; Bright, R. M.; Brown, K. R.; Freeman, R. G.; Fox, A. P.; Keating, C. D.; Musick, M. D.; Natan, M. J. Two-Dimensional Arrays of Colloidal Gold Particles: a Flexible Approach to Macroscopic Metal Surfaces. *Langmuir* **1996**, *12*, 2353–2361.
(45) Peng, Z.; Liu, H. Bottom-Up Nanofabrication Using DNA Nanostructures. *Chem. Mater.* **2016**, *28*, 1012–1021.
(46) Pinheiro, A. V.; Han, D.; Shih, W. M.; Yan, H. Challenges and Opportunities for Structural DNA Nanotechnology. *Nature Nanotechnology* **2011**, *6*, 763–772.
(47) Park, M.; Harrison, C.; Chaikin, P. M.; Register, R. A.; Adamson, D. H. Block Copolymer Lithography: Periodic Arrays of $\sim 10^{11}$ Holes in 1 Square Centimeter. *Science* **1997**, *276*, 1401–1404.
(48) Darling, S. B. Directing the Self-Assembly of Block Copolymers. *Progress in Polymer Science* **2007**, *32*, 1152–1204.

(49) Hawker, C. J.; Russell, T. P. Block Copolymer Lithography: Merging “Bottom-Up” with ‘Top-Down’ Processes. *MRS bulletin* **2005**, *30*, 952–966.
(50) Cheng, J. Y.; Ross, C. A.; Smith, H. I.; Thomas, E. L. Templated Self-Assembly of Block Copolymers: Top-Down Helps Bottom-Up. *Adv. Mater.* **2006**, *18*, 2505–2521.
(51) Förster, S. Amphiphilic Block Copolymers for Templating Applications. *Colloid Chemistry 1* **2003**, *226*, 1–28.
(52) Orilall, M. C.; Wiesner, U. Block Copolymer Based Composition and Morphology Control in Nanostructured Hybrid Materials for Energy Conversion and Storage: Solar Cells, Batteries, and Fuel Cells. *Chem. Soc. Rev.* **2011**, *40*, 520–535.
(53) Brinker, C. J.; Lu, Y. F.; Sellinger, A.; Fan, H. Y. Evaporation-Induced Self-Assembly: Nanostructures Made Easy. *Adv. Mater.* **1999**, *11*, 579–585.
(54) Lohmüller, T.; Aydin, D.; Schwieder, M.; Morhard, C.; Louban, I.; Pacholski, C.; Spatz, J. P. Nanopatterning by Block Copolymer Micelle Nanolithography and Bioinspired Applications. *Biointerphases* **2011**, *6*, MR1–MR12.
(55) Polleux, J.; Rasp, M.; Louban, I.; Plath, N.; Feldhoff, A.; Spatz, J. P. Benzyl Alcohol and Block Copolymer Micellar Lithography: a Versatile Route to Assembling Gold and in SituGenerated Titania Nanoparticles Into Uniform Binary Nanoarrays. *ACS Nano* **2011**, *5*, 6355–6364.
(56) Lopes, W. A.; Jaeger, H. M. Hierarchical Self-Assembly of Metal Nanostructures on Diblock Copolymer Scaffolds. *Nature* **2001**, *13*, 1174–1178.
(57) Cheng, J. Y.; Ross, C. A.; Chan, V.; Thomas, E. L.; Lammertink, R.; Vancso, G. J. Formation of a Cobalt Magnetic Dot Array via Block Copolymer Lithography. *Adv. Mater.* **2001**, *13*, 1174–1178.
(58) Moon, H.-S.; Kim, J. Y.; Jin, H. M.; Lee, W. J.; Choi, H. J.; Mun, J. H.; Choi, Y. J.; Cha, S. K.; Kwon, S. H.; Kim, S. O. Atomic Layer Deposition Assisted Pattern Multiplication of Block Copolymer Lithography for 5 Nm Scale Nanopatterning. *Adv. Funct. Mater.* **2014**, *24*, 4343–4348.
(59) Wang, Y.; Becker, M.; Wang, L.; Liu, J.; Scholz, R.; Peng, J.; Gösele, U.; Christiansen, S.; Kim, D. H.; Steinhart, M. Nanostructured Gold Films for SERS by Block Copolymer-Templated Galvanic Displacement Reactions. *Nano Lett.* **2009**, *9*, 2384–2389.
(60) Aizawa, M.; Buriak, J. M. Block Copolymer Templated Chemistry for the Formation of Metallic Nanoparticle Arrays on Semiconductor Surfaces. *Chem. Mater.* **2007**, *19*, 5090–5101.
(61) Porter, L. A.; Choi, H. C.; Schmeltzer, J. M.; Ribbe, A. E.; Elliott, L. C. C.; Buriak, J. M. Electroless Nanoparticle Film Deposition Compatible with Photolithography, Microcontact Printing, and Dip-Pen Nanolithography Patterning Technologies. *Nano Lett.* **2002**, *2*, 1369–1372.
(62) Vukovic, I.; ten Brinke, G.; Loos, K. Block Copolymer Template-Directed Synthesis of Well-Ordered Metallic Nanostructures. *Polymer* **2013**, *54*, 2591–2605.

(63) Thurn-Albrecht, T.; Schotter, J.; Kästle, G. A.; Emley, N.; Shibauchi, T.; Krusin-Elbaum, L.; Guarini, K.; Black, C. T.; Tuominen, M. T.; Russell, T. P. Ultrahigh-Density Nanowire Arrays Grown in Self-Assembled Diblock Copolymer Templates. *Science* **2000**, *290*, 2126–2129.

(64) Lohmueller, T.; Bock, E.; Spatz, J. P. Synthesis of Quasi-Hexagonal Ordered Arrays of Metallic Nanoparticles with Tuneable Particle Size. *Adv. Mater.* **2008**, *20*, 2297–2302.

(65) Zhu, M.; Baffou, G.; Meyerbröker, N.; Polleux, J. Micropatterning Thermoplasmonic Gold Nanoarrays to Manipulate Cell Adhesion. *ACS Nano* **2012**, *6*, 7227–7233.

(66) Ullrich, S.; Scheeler, S. P.; Pacholski, C.; Spatz, J. P.; Kudera, S. Formation of Large 2D Arrays of Shape-Controlled Colloidal Nanoparticles at Variable Interparticle Distances. *Part. Part. Syst. Charact.* **2012**, *30*, 102–108.

(67) Lee, W.; Lee, S. Y.; Briber, R. M.; Rabin, O. Self-Assembled SERS Substrates with Tunable Surface Plasmon Resonances. *Adv. Funct. Mater.* **2011**, *21*, 3424–3429.

(68) Mueller, M.; Tebbe, M.; Andreeva, D. V.; Karg, M.; Alvarez Puebla, R. A.; Pazos Perez, N.; Fery, A. Large-Area Organization of pNIPAM-Coated Nanostars as SERS Platforms for Polycyclic Aromatic Hydrocarbons Sensing in Gas Phase. *Langmuir* **2012**, *28*, 9168–9173.

(69) Yap, F. L.; Thoniyot, P.; Krishnan, S.; Krishnamoorthy, S. Nanoparticle Cluster Arrays for High-Performance SERS Through Directed Self-Assembly on Flat Substrates and on Optical Fibers. *ACS Nano* **2012**, *6*, 2056–2070.

(70) Yu, Q.; Johnson, L. M.; López, G. P. Nanopatterned Polymer Brushes for Triggered Detachment of Anchorage-Dependent Cells. *Adv. Funct. Mater.* **2014**, *24*, 3751–3759.

(71) Rolli, C. G.; Nakayama, H.; Yamaguchi, K.; Spatz, J. P.; Kemkemer, R.; Nakanishi, J. Switchable Adhesive Substrates: Revealing Geometry Dependence in Collective Cell Behavior. *Biomaterials* **2012**, *33*, 2409–2418.

(72) Glass, R.; Möller, M.; Spatz, J. P. Block Copolymer Micelle Nanolithography. *Nanotechnology* **2003**, *14*, 1153–1160.

(73) Glass, R.; Arnold, M.; Cavalcanti-Adam, E. A.; Blümmel, J.; Haferkemper, C.; Dodd, C.; Spatz, J. P. Block Copolymer Micelle Nanolithography on Non-Conductive Substrates. *New Journal of Physics* **2004**, *6*, 101–101.

(74) Chen, J.; Mela, P.; Möller, M.; Lensen, M. C. Microcontact Deprinting: a Technique to Pattern Gold Nanoparticles. *ACS Nano* **2009**, *3*, 1451–1456.

(75) Aydin, D.; Schwieder, M.; Louban, I.; Knoppe, S.; Ulmer, J.; Haas, T. L.; Walczak, H.; Spatz, J. P. Micro-Nanostructured Protein Arrays: a Tool for Geometrically Controlled Ligand Presentation. *Small* **2009**, *5*, 1014–1018.

(76) Müller, M. B.; Kuttner, C.; König, T. A. F.; Tsukruk, V. V.; Förster, S.; Karg, M.; Fery, A. Plasmonic Library Based on Substrate-Supported Gradiential Plasmonic Arrays. *ACS Nano* **2014**, *8*, 9410–9421.

(77) Wang, L.; Montagne, F.; Hoffmann, P.; Heinzelmann, H.; Pugin, R. Hierarchical Positioning of Gold Nanoparticles Into Periodic Arrays Using Block Copolymer Nanoring Templates. *Journal of Colloid and Interface Science* **2011**, *356*, 496–504.

(78) Fontana, J.; Livenere, J.; Bezares, F. J.; Caldwell, J. D.; Rendell, R.; Ratna, B. R. Large Surface-Enhanced Raman Scattering From Self-Assembled Gold Nanosphere Monolayers. *Appl. Phys. Lett.* **2013**, *102*, 201606.
(79) Li, M.; Ober, C. K. Block Copolymer Patterns and Templates. *Materials Today* **2006**, *9*, 30–39.
(80) Stoykovich, M. P.; Nealey, P. F. Block Copolymers and Conventional Lithography. *Materials Today* **2006**, *9*, 20–29.
(81) Kumar, S.; Yang, H.; Zou, S. Seed-Mediated Growth of Uniform Gold Nanoparticle Arrays. *J. Phys. Chem. C* **2007**, *111*, 12933–12938.
(82) Osinkina, L.; Lohmüller, T.; Jäckel, F.; Feldmann, J. Synthesis of Gold Nanostar Arrays as Reliable, Large-Scale, Homogeneous Substrates for Surface-Enhanced Raman Scattering Imaging and Spectroscopy. *J. Phys. Chem. C* **2013**, *117*, 22198–22202.
(83) Mieszawska, A. J.; Slawinski, G. W.; Zamborini, F. P. Directing the Growth of Highly Aligned Gold Nanorods Through a Surface Chemical Amidation Reaction. *J. Am. Chem. Soc.* **2006**, *128*, 5622–5623.
(84) Mahmoud, M. A.; O'Neil, D.; El-Sayed, M. A. Hollow and Solid Metallic Nanoparticles in Sensing and in Nanocatalysis. *Chem. Mater.* **2014**, *26*, 44–58.
(85) Yan, B.; Boriskina, S. V.; Reinhard, B. M. Design and Implementation of Noble Metal Nanoparticle Cluster Arrays for Plasmon Enhanced Biosensing. *J. Phys. Chem. C* **2011**, *115*, 24437–24453.
(86) Baffou, G.; Quidant, R. Thermo-Plasmonics: Using Metallic Nanostructures as Nano-Sources of Heat. *Laser & Photonics Reviews* **2013**, *7*, 171–187.
(87) Homola, J.; Yee, S. S.; Gauglitz, G. Surface Plasmon Resonance Sensors: Review. *Sensors and Actuators B-Chemical* **1999**, *54*, 3–15.
(88) Zeng, S.; Yong, K.-T.; Roy, I.; Dinh, X.-Q.; Yu, X.; Luan, F. A Review on Functionalized Gold Nanoparticles for Biosensing Applications. *Plasmonics* **2011**, *6*, 491–506.
(89) Liu, S.; Tang, Z. Nanoparticleassemblies for Biological and Chemical Sensing. *J. Mater. Chem.* **2010**, *20*, 24–35.
(90) de Aberasturi, D. J.; Serrano-Montes, A. B.; Liz-Marzán, L. M. Modern Applications of Plasmonic Nanoparticles: From Energy to Health. *Advanced Optical Materials* **2015**, *3*, 602–617.
(91) Baffou, G.; Polleux, J.; Rigneault, H.; Monneret, S. Super-Heating and Micro-Bubble Generation Around Plasmonic Nanoparticles Under Cw Illumination. *J. Phys. Chem. C* **2014**, *118*, 4890–4898.
(92) Baffou, G.; Quidant, R. Nanoplasmonics for Chemistry. *Chem. Soc. Rev.* **2014**, *43*, 3898–3907.
(93) Kale, M. J.; Avanesian, T.; Christopher, P. Direct Photocatalysis by Plasmonic Nanostructures. *ACS Catal.* **2014**, *4*, 116–128.
(94) Zhang, X.; Chen, Y. L.; Liu, R.-S.; Tsai, D. P. Plasmonic Photocatalysis. *Rep. Prog. Phys.* **2013**, *76*, 046401.
(95) Wang, C.; Astruc, D. Nanogold Plasmonic Photocatalysis for Organic Synthesis and Clean Energy Conversion. *Chem. Soc. Rev.* **2014**, *43*, 7188–7216.

(96) Vázquez-Vázquez, C.; Vaz, B.; Giannini, V.; Pérez-Lorenzo, M.; Alvarez Puebla, R. A.; Correa-Duarte, M. A. Nanoreactors for Simultaneous Remote Thermal Activation and Optical Monitoring of Chemical Reactions. *J. Am. Chem. Soc.* **2013**, *135*, 13616–13619.
(97) Yen, C.-W.; El-Sayed, M. A. Plasmonic Field Effect on the Hexacyanoferrate (III)-Thiosulfate Electron Transfer Catalytic Reaction on Gold Nanoparticles: Electromagnetic or Thermal? *J. Phys. Chem. C* **2009**, *113*, 19585–19590.
(98) Qiu, J.; Wei, W. D. Surface Plasmon-Mediated Photothermal Chemistry. *J. Phys. Chem. C* **2014**, *118*, 20735–20749.
(99) Xiao, M.; Jiang, R.; Wang, F.; Fang, C.; Wang, J.; Yu, J. C. Plasmon-Enhanced Chemical Reactions. *J. Mater. Chem. A* **2013**, *1*, 5790–5805.
(100) Cao, L.; Barsic, D. N.; Guichard, A. R.; Brongersma, M. L. Plasmon-Assisted Local Temperature Control to Pattern Individual Semiconductor Nanowires and Carbon Nanotubes. *Nano Lett.* **2007**, *7*, 3523–3527.
(101) Hwang, D. J.; Ryu, S.-G.; Grigoropoulos, C. P. Multi-Parametric Growth of Silicon Nanowires in a Single Platform by Laser-Induced Localized Heat Sources. *Nanotechnology* **2011**, *22*, 385303.
(102) Boyd, D. A.; Greengard, L.; Brongersma, M.; El-Naggar, M. Y.; Goodwin, D. G. Plasmon-Assisted Chemical Vapor Deposition. *Nano Lett.* **2006**, *6*, 2592–2597.
(103) Hung, W. H.; Hsu, I.-K.; Bushmaker, A.; Kumar, R.; Theiss, J.; Cronin, S. B. Laser Directed Growth of Carbon-Based Nanostructures by Plasmon Resonant Chemical Vapor Deposition. *Nano Lett.* **2008**, *8*, 3278–3282.
(104) Chen, X.; Zhu, H. Y.; Zhao, J. C.; Zheng, Z. F.; Gao, X. P. Visible-Light-Driven Oxidation of Organic Contaminants in Air with Gold Nanoparticle Catalysts on Oxide Supports. *Angew. Chem. Int. Ed.* **2008**, *120*, 5353–5356.
(105) Hung, W. H.; Aykol, M.; Valley, D.; Hou, W.; Cronin, S. B. Plasmon Resonant Enhancement of Carbon Monoxide Catalysis. *Nano Lett.* **2010**, *10*, 1314–1318.
(106) Adleman, J. R.; Boyd, D. A.; Goodwin, D. G.; Psaltis, D. Heterogenous Catalysis Mediated by Plasmon Heating. *Nano Lett.* **2009**, *9*, 4417–4423.
(107) Fasciani, C.; Alejo, C. J. B.; Grenier, M.; Netto-Ferreira, J. C.; Scaiano, J. C. High-Temperature Organic Reactions at Room Temperature Using Plasmon Excitation: Decomposition of Dicumyl Peroxide. *Org. Lett.* **2011**, *13*, 204–207.
(108) Feng, S.; Xu, R. New Materials in Hydrothermal Synthesis. *Acc. Chem. Res.* **2001**, *34*, 239–247.
(109) Shanmugam, V.; Selvakumar, S.; Yeh, C.-S. Near-Infrared Light-Responsive Nanomaterials in Cancer Therapeutics. *Chem. Soc. Rev.* **2014**, *43*, 6254–6287.
(110) Jain, P. K.; El-Sayed, I. H.; El-Sayed, M. A. Au Nanoparticles Target Cancer. *Nano Today* **2007**, *2*, 18–29.
(111) Turko, N. A.; Barnea, I.; Blum, O.; Korenstein, R.; Shaked, N. T. Detection and Controlled Depletion of Cancer Cells Using Photothermal Phase Microscopy. *J. Biophoton.* **2014**, *8*, 755–763.
(112) Turko, N. A.; Peled, A.; Shaked, N. T. Wide-Field Interferometric Phase Microscopy with Molecular Specificity Using Plasmonic Nanoparticles. *J. Biomed. Opt* **2013**, *18*, 111414.

(113) Berciaud, S.; Cognet, L.; Blab, G. A.; Lounis, B. Photothermal Heterodyne Imaging of Individual Nonfluorescent Nanoclusters and Nanocrystals. *Phys. Rev. Lett.* **2004**, *93*, 257402.
(114) Choi, W. I.; Sahu, A.; Kim, Y. H.; Tae, G. Photothermal Cancer Therapy and Imaging Based on Gold Nanorods. *Ann Biomed Eng* **2011**, *40*, 534–546.
(115) Nakatsuji, H.; Numata, T.; Morone, N.; Kaneko, S.; Mori, Y.; Imahori, H.; Murakami, T. Thermosensitive Ion Channel Activation in Single Neuronal Cells by Using Surface-Engineered Plasmonic Nanoparticles. *Angew. Chem.* **2015**, *127*, 11891–11895.
(116) Son, J. H.; Cho, B.; Hong, S.; Lee, S. H.; Hoxha, O.; Haack, A. J.; Lee, L. P. Ultrafast Photonic PCR. *Light Sci Appl* **2015**, *4*, e280.
(117) Grier, D. G. A Revolution in Optical Manipulation. *Nature* **2003**, *424*, 810–816.
(118) Moffitt, J. R.; Chemla, Y. R.; Smith, S. B.; Bustamante, C. Recent Advances in Optical Tweezers. *Annu. Rev. Biochem.* **2008**, *77*, 205–228.
(119) Piazza, R. Thermophoresis: Moving Particles with Thermal Gradients. *Soft Matter* **2008**, *4*, 1740–1744.
(120) Braun, D.; Libchaber, A. Trapping of DNA by Thermophoretic Depletion and Convection. *Phys. Rev. Lett.* **2002**, *89*, 188103.
(121) Jiang, H.-R.; Wada, H.; Yoshinaga, N.; Sano, M. Manipulation of Colloids by a Nonequilibrium Depletion Force in a Temperature Gradient. *Phys. Rev. Lett.* **2009**, *102*, 208301.
(122) Duhr, S.; Braun, D. Optothermal Molecule Trapping by Opposing Fluid Flow with Thermophoretic Drift. *Phys. Rev. Lett.* **2006**, *97*, 038103.
(123) Maeda, Y. T.; Tlusty, T. Effects of Long DNA Folding and Small RNA Stem–Loop in Thermophoresis. In; 2012; Vol. 109, pp. 17972–17977.
(124) Weinert, F. M.; Braun, D. An Optical Conveyor for Molecules. *Nano Lett.* **2009**, *9*, 4264–4267.
(125) Duhr, S.; Braun, D. Two-Dimensional Colloidal Crystals Formed by Thermophoresis and Convection. *Appl. Phys. Lett.* **2005**, *86*, 131921–131921.
(126) Huang, L.; Maerkl, S. J.; Martin, O. J. F. Integration of Plasmonic Trapping in a Microfluidic Environment. *Optics Express* **2009**, *17*, 6018–6024.
(127) Kang, Z.; Chen, J.; Wu, S.-Y.; Ho, H.-P. Plasmonic Absorption Activated Trapping and Assembling of Colloidal Crystals with Non-Resonant Continuous Gold Films. *RSC Adv.* **2015**, *5*, 105409–105415.
(128) Li, Y.; Xu, L.; Li, B. Gold Nanorod-Induced Localized Surface Plasmon for Microparticle Aggregation. *Appl. Phys. Lett.* **2012**, *101*, 053118.
(129) Braun, M.; Cichos, F. Optically Controlled Thermophoretic Trapping of Single Nano-Objects. *ACS Nano* **2013**, *7*, 11200–11208.
(130) Chen, Y.-H.; Chang, S.-H.; Wang, T.-J.; Wang, I.-J.; Young, T.-H. Cell Fractionation on pH-Responsive Chitosan Surface. *Biomaterials* **2013**, *34*, 854–863.
(131) Inaba, R.; Khademhosseini, A.; Suzuki, H.; Fukuda, J. Electrochemical Desorption of Self-Assembled Monolayers for Engineering Cellular Tissues. *Biomaterials* **2009**, *30*, 3573–3579.

(132) Yamaguchi, S.; Yamahira, S.; Kikuchi, K.; Sumaru, K.; Kanamori, T.; Nagamune, T. Photocontrollable Dynamic Micropatterning of Non-Adherent Mammalian Cells Using a Photocleavable Poly(Ethylene Glycol) Lipid. *Angew. Chem. Int. Ed.* **2011**, *51*, 128–131.
(133) Kolesnikova, T. A.; Kohler, D.; Skirtach, A. G.; Möhwald, H. Laser-Induced Cell Detachment, Patterning, and Regrowth on Gold Nanoparticle Functionalized Surfaces. *ACS Nano* **2012**, *6*, 9585–9595.
(134) Giner-Casares, J. J.; Henriksen-Lacey, M.; García, I.; Liz-Marzán, L. M. Plasmonic Surfaces for Cell Growth and Retrieval Triggered by Near-Infrared Light. *Angew. Chem.* **2015**, *128*, 986–990.
(135) Liu, Z.; Liu, Y.; Chang, Y.; Seyf, H. R.; Henry, A.; Mattheyses, A. L.; Yehl, K.; Zhang, Y.; Huang, Z.; Salaita, K. Nanoscale Optomechanical Actuators for Controlling Mechanotransduction in Living Cells. *Nature Methods* **2015**, *13*, 143–146.
(136) Fenno, L.; Yizhar, O.; Deisseroth, K. The Development and Application of Optogenetics. *Annu Rev Neurosci* **2011**, *34*, 389–412.
(137) Wu, Y. I.; Frey, D.; Lungu, O. I.; Jaehrig, A.; Schlichting, I.; Kuhlman, B.; Hahn, K. M. A Genetically Encoded Photoactivatable Rac Controls the Motility of Living Cells. *Nature* **2009**, *461*, 104–108.
(138) Kundrat, F.; Baffou, G.; Polleux, J. Shaping and Patterning Gold Nanoparticles via Micelle Templated Photochemistry. *Nanoscale* **2015**, *7*, 15814–15821.

5. Acknowledgements

This work would not have been possible without help and support of many people in and outside the lab to all of whom I want to thank here:

First and foremost I want to thank Dr. Julien Polleux, my supervisor, for giving me the opportunity to work on this fascinating project. I enjoyed a lot working at the interface of many scientific disciplines including material science, nanotechnology and biology and its various challenges motivated me throughout this work. I would like to thank him for all his support, excellent supervision and constant encouragement over the years. He was always open for discussions and advice and taught me to be critical about my work. Also, I want to express my gratitude for his great patience with optimizing my presentations and talks and for the intensive revision of this thesis.

Second, I would like to express my deep gratitude to Prof. Dr. Reinhard Fässler, for mentoring this thesis as my doctor father and making this thesis possible. In addition, I want to thank him for his generous support and scientific advices. Also, I am much obliged for the possibility to have performed my study in such excellent conditions.

Furthermore, I want to appreciate my collaborators Jacob Verghese for his help and fruitful discussions and especially Dr. Guillaume Baffou, for essential contributions for the work presented in this thesis as well as productive discussions.

Also, I would like to acknowledge Dr. Anette Müller-Taubenberger, Prof. Kay-E. Gottschalk and Prof. Michael Sixt, the members of my thesis advisory committee, for the agreement to evaluate my work and supporting it with ideas and motivating discussions.

Moreover, I would like to thank Prof. Dieter Braun, who agreed to be the second referee of my thesis as well as the other members of my thesis committee Prof. Gerhard Winter, Prof. Achim Hartschuh, Dr. habil. Dina Fattakhova-Rohlfing and Prof. Ernst Wagner for their willingness to evaluate my thesis.

Besides, I am grateful for all former and present members of the department, for all the help I received along the way. I am especially grateful to Valeria Soberón, Maria Benito-Jardón, Georgina Coló, Marina Theodosiou, Valeria Samarelli and Patricia Kammerer, who have become good friends over time. I want to thank them for fruitful scientific discussions as well as sharing the good and the bad of every day life in the lab and also for all the fun we had together in and outside of the lab.

Additionally, I want to appreciate Klaus Weber, Ines Lach-Kusevic, Lidia Wimmer and Dr. Armin Lambacher for all the technical and administrative support.

Finally, my very special thanks go to my parents, my sister and my grandmother Marlitt, for their love and for the continuous support and encouragement during all the years of my studies, and before.

6. Curriculum Vitae

Franziska Kundrat (MSc.)

Klenzestr. 75, 80469Munich
franziska_kundrat@yahoo.de, +4917663446340

Personal Details

Date of birth: 16/08/1987
Nationality: German

Higher Education

10/2012-10/2016 **Doctoral Studies** in Biochemistry
Max Planck Institute for Biochemistry, Department for Molecular Medicine
Topic: *''Micelle Templated Photochemistry, a New Approach to Fabricate Functional Photothermal Gold Nanoarrays "*
Supervisors: Dr. Julien Polleux, Prof. Dr. Reinhard Fässler

10/2010-09/2012 **Master of Science** in Chemistry
University of Regensburg, Germany
Majors: Bioanalytics, Orgnic Chemistry, Biochemistry

10/2007 – 02/2011 **Bachelorof Science** in Chemistry
University of Regensburg, Germany

Working Experience

02/2012-09/2012 **ScientificResearch Assistant**
Fraunhofer Research Institution for Modular Solid State-Technologies EMFT, Workgroup Sensor materials, Regensburg

Fellowship

10/2012-10/2013 **Graduate Program of CRC 941**, Integrated Research Training Group, IRTG 941

Publication

01/9/2015 **Kundrat, F**., Baffou, G. & Polleux, J.
Shaping and patterning gold nanoparticles via micelle template photochemistry, *Nanoscale*

06/7/2016 Robert H, **Kundrat F**, Bermúdez-Ureña E, Rigneault H, Monneret S, Quidant R, Polleux J, Baffou G.
Light-Assisted Solvothermal Chemistry Using Plasmonic Nanoparticles, *ACS Omega*

Presentation and Communication Skills

03-06/11/2014, 21-24/10/2013	**Oral presentations** and **chairing** in annual retreats of IRTG 941 (Germany, Italy)
20-23/3/2013	**Poster presentation** in annual retreat of CRC 941 (Austria)

Supervision and Project Management

20-23/04/2015, 23-25/04/2014, 06-10/05/2013	**Practical course biochemistry** BC1, LMU 1 week, 8 students Supervision in the lab, online-test analysis and protocol-corrections
25/07/2014	MPI Summer Party, **logistics** and **poster-design**
08/11/2014	MPI Open Day, escort of **guided tours**
20/11/2014	MPI Get Together, **logistics** and **catering**

Languages

German	native speaker
English	fluent
Spanish	elementary (Unicert® I, course 1/2)
Latinum	

Computer Packages

General	Microsoft Office (Excel, Word, PowerPoint), Keynote
Data-analysis	ImageJ, Origin, MestReNova NMR
Graphic-design	Adobe Photoshop& Illustrator, ChemDraw

Workshops

17-18/02/2014	**Applied Statistics** for Molecular Biologists (IRTG, Tobias Straub)
13-14/06/2013	**Scientific Writing** (IRTG, Mary Scholz)

7. Appendix

In the following Manuscripts I and II are reprinted.

7.1. Manuscript I

Shaping and Patterning Gold Nanoparticles *via* Micelle Templated Photochemistry

This study was the main focus of my thesis. I designed and performed most of the experiments and analyzed them under the supervision of J. Polleux, who initiated the project. G. Baffou performed and analyzed the thermal measurements.

Published as:
Kundrat F, Baffou G, Polleux J. Shaping and patterning gold nanoparticles via micelle templated photochemistry. *Nanoscale*, 2015, 7, 15814-15821.

Nanoscale

PAPER

View Article Online
View Journal

Cite this: DOI: 10.1039/c5nr04751j

Shaping and patterning gold nanoparticles *via* micelle templated photochemistry†

F. Kundrat,[a] G. Baffou[b] and J. Polleux*[a,c]

Received 15th July 2015,
Accepted 29th August 2015

DOI: 10.1039/c5nr04751j

www.rsc.org/nanoscale

Shaping and positioning noble metal nanostructures are essential processes that still require laborious and sophisticated techniques to fabricate functional plasmonic interfaces. The present study reports a simple photochemical approach compatible with micellar nanolithography and photolithography that enables the growth, arrangement and shaping of gold nanoparticles with tuneable plasmonic resonances on glass substrates. Ultraviolet illumination of surfaces coated with gold-loaded micelles leads to the formation of gold nanoparticles with micro/nanometric spatial resolution without requiring any photosensitizers or photoresists. Depending on the extra-micellar chemical environment and the illumination wavelength, block copolymer micelles act as reactive and light-responsive templates, which enable to grow gold deformed nanoparticles (potatoids) and nanorings. Optical characterization reveals that arrays of individual potatoids and rings feature a localized plasmon resonance around 600 and 800 nm, respectively, enhanced photothermal properties and high temperature sustainability, making them ideal platforms for future developments in nanochemistry and biomolecular manipulation controlled by near-infrared-induced heat.

Introduction

Noble metal nanoparticles significantly moved forward the development of nanosciences over the last two decades due to their remarkable optical properties.[1] In particular, gold nanoparticles feature localized plasmon resonances that enhance light absorption and scattering from visible to infrared frequencies.[2] Although colloidal gold have been used since ancient times, the establishment of reproducible synthetic methods recently allowed understanding the shape-dependent optical properties of nanoparticles.[3] Approaches to obtain extended and uniform distributions of nanoparticles on planar substrates attracted a lot of attention too, as it offers a convenient configuration for fundamental optical studies[4] and applications in nanocatalysis,[5] biosensing[6,7] and photothermy.[8,9] It is common to fabricate nanoparticle monolayers using physical means,[10–12] but most approaches still have significant limitations in simplifying multi-step procedures and using benchtop facilities. The simple deposition or immobilization of dispersed nano-objects constitutes a scalable and cost-effective way to fabricate plasmonic substrates. However, such approaches do not allow the uniform assembly of particles over macroscopic areas.[13–20]

Block-copolymer micellar lithography (BCML) has been recognized as a facile method for generating uniform and regular arrays of nanoparticles with sub-30 nm resolution over arbitrarily large areas.[21,22] Amphiphilic diblock copolymers undergo microphase segregation in solvents selective for one of the two blocks, resulting in the formation of supramolecular structures.[23] It is simple to simultaneously transfer and organize these structures from solution to substrates *via* evaporation-induced self-assembly.[24] Upon deposition, the extended and ordered domains of self-assembled block copolymer molecules can be used as a template to selectively control the deposition of inorganic nanoparticles[18,25,26] and molecular precursors. Many approaches such as thermal evaporation,[27] reactive ion etching,[28] electrochemical plating,[29,30] atomic layer deposition,[31] galvanic displacement,[32–34] sol–gel chemistry,[35,36] and plasma reduction[36–40] have been combined with BCML for the fabrication of quasi-hexagonally organized nanodots and parallel nanowires of various compositions. Especially for gold, these strategies have been successful to design plasmon-based sensors[18,41] and bioactive substrates.[42,43] However, tuning the optical properties of substrates made by BCML is difficult as spherical gold

[a]Max Planck Institute of Biochemistry, Department of Molecular Medicine, 82152 Martinsried, Germany. E-mail: polleux@biochem.mpg.de
[b]Fresnel Institute UMR 7249, CNRS, Aix-Marseille Université, Ecole Centrale Marseille, 13013 Marseille, France
[c]Center for NanoScience, Ludwig Maximilian University, 80799 Munich, Germany

†Electronic supplementary information (ESI) available: Additional SEM, TEM and extinction measurements further describe the mechanism of the reported photochemical approach. See DOI: 10.1039/c5nr04751j

nanoparticles only absorb at around 520 nm and micrometre-long nanowires display a broad longitudinal plasmon resonance in the infrared due to their polydispersity in length. In order to tune the optical properties of the substrates within the visible and near-infrared spectral range, adjusting gold nanoparticle morphology is necessary. For this purpose, several groups used immobilized gold nanoparticles acting as seeds to mediate the growth of anisotropic nanostructures.[44–47] Nevertheless, this strategy only leads to the non-uniform formation of nanoparticles of different morphologies and sizes, as it is not possible to control the crystallographic orientation of the initial metal seeds. Recently, urchin-shaped gold nanoparticles were successfully grown from arrays of spherical nanoparticles.[48] Although they proved to be reliable substrates for Raman imaging and spectroscopy, the surface plasmon resonance of such nanostructures was neither characterized nor shown to be tuneable.

In this article, we report a straightforward and cost-effective photochemical approach suited to fabricate uniform and robust nanoparticle arrays with adjustable plasmonic resonances on arbitrarily large glass substrates. We first describe the method to photochemically synthesize gold nanoparticles on polymer-coated surfaces. Next, we show that nanoparticle growth can be resolved at the nanoscale by using block copolymer micellar monolayers as reactive and light-responsive templates. In particular, we describe the preparation of quasi-hexagonally organized randomly shaped nanoparticles (hereinafter termed potatoids) and nanorings. Finally, we characterize their optical and photothermal properties in the context of future applications in plasmon-assisted chemistry.

Experimental

Fabrication of gold nanoparticles on homopolymer thin films

Polystyrene (MW 192 000, PS_{1846}, Sigma-Aldrich) and poly(2-vinylpyridine) (MW 159 000, $P2VP_{1507}$, Sigma-Aldrich) were dissolved at a concentration of 2 mg mL^{-1} in *o*-xylene and chloroform, respectively. Glass coverslips (Carl Roth) were cleaned in a piranha solution for at least 2 hours, extensively rinsed with MilliQ water and dried under a stream of nitrogen. Homopolymer thin films were prepared by dip-coating a glass coverslip into the previously prepared solutions with a constant velocity equal to 30 mm min^{-1}. A 2.3 μL drop of aqueous solution of gold chloride (1 wt%, 2.5 mM $HAuCl_4$, Sigma-Aldrich) was placed onto a UV-transparent quartz coverslip (Jena Compugraphics). The drop was cautiously flattened with the homopolymer coated glass coverslip while preventing the formation of air bubbles, resulting in a spacing of about 10 μm between both interfaces. The sandwiched system was then exposed to deep UV light using a low-pressure dual emission mercury lamp (Heraeus Noblelight GmbH, NIQ 60/35 XL long-life lamp, 254 and 185 nm with an output of 20 and 5 W, respectively). To remove the coverslip from the quartz, the system was placed in a plastic dish filled with water. Once lifted by water, the coverslip is rinsed with water and dried with nitrogen.

Fabrication of gold nanoparticle arrays with various particle morphologies

Polystyrene(102 000)-*block*-poly(2-vinylpyridine)(97 000) (PS_{980}-*b*-$P2VP_{923}$) from Polymer Source Inc. was dissolved at room temperature in anhydrous *o*-xylene (Sigma-Aldrich) at a concentration of 1.7 mg mL^{-1} in a sealed glass vessel. The solution was then stirred for 2 days. Hydrogen tetrachloroaurate(III) trihydrate ($HAuCl_4 \cdot 3H_2O$, Sigma-Aldrich) was added to the polymer solution, stirred for 2 days and filtered. The quantity of gold precursor was calculated relative to the number of P2VP units with a loading parameter (L) equal to 0.75, *i.e.* 3 molecules of $HAuCl_4$ for 4 vinylpyridine monomers. Gold-loaded micellar monolayers were prepared by dip-coating a glass coverslip into the previously prepared solutions with a constant velocity equal to 24 mm min^{-1}. A 2.3 μL drop of water or gold aqueous solution was placed onto a UV-transparent quartz coverslip or a photomask (Jena Compugraphics). The drop was cautiously flattened with the coated glass coverslip. The sandwiched system was then exposed to deep UV light using either a low-pressure dual emission mercury lamp or a monochromatic lamp (NNI 65/35 XL, 254 nm – 20 W) at 5 cm distance for 4 min. To remove the coverslip from the quartz, the system was placed in a plastic dish filled with water. Once lifted by water, the coverslip is rinsed with water and transferred in a 10 mL aqueous solution containing ethanolamine (2 mM, Sigma-Aldrich) and $KAuCl_4$ (0.1 wt%, *i.e.* 0.25 mM, Sigma-Aldrich) in order to enlarge the photo-deposited gold nanoparticles. To remove the organic compounds, the processed glass coverslip was exposed to oxygen plasma (1 mbar, Power 65%, 1 h, Modele Femto, Diener). Scanning electron measurements were performed with a Dual Beam™ (FIB/SEM) instrument (Quanta 3D FEG, FEI, Hillsboro). The absorbance spectra were acquired in air with a UV Spectrometer PerkinElmer Lambda 19.

Thermal measurements using TIQSI

Temperature measurements were performed by wavefront sensing using quadriwave shearing interferometry (QSI). Using this technique, a plane optical wavefront crosses the region of interest and undergoes a distorsion due to the thermal-induced variation of the refractive index of the medium (water in this article). This wavefront distorsion is imaged quantitatively using a QSI wavefront analyser. The source was a collimated light emitted diode from *Thorlabs* (reference no M625L2-C1) whose emitting spectrum spans from 600 to 650 nm. The QSI wavefront analyser was purchased from the *Phasics SA* company (reference name: Sid4Bio). Each image presented in this work is the result of the average of 30 wavefront images, corresponding to a whole acquisition time of around 3 seconds.

Results and discussion

A simple photochemical approach to grow gold nanoparticle monolayers

Among the large variety of synthetic methods that allow the preparation of inorganic nanoparticles, photochemical

approaches have been widely used to establish non-toxic and waste free chemical reactions with high spatial resolution in various environments such as glasses, polymer films, micelles, emulsions, biomolecules and living cells.[49–51] Such synthetic pathways often involve the use of photosensitizing molecules that generate radicals necessary for the effective reduction of metallic precursors. Radical formation can either take place directly upon photo-induced bond cleavage of the photosensitizer or indirectly upon photo-excitation of the sensitizers able to abstract the hydrogen atoms of donor molecules (H-donors), which turn into reducing species.[49] To simplify the generation of reducing radicals, Scaiano and coworkers recently showed that tetrachloroaurate anions $[AuCl_4]^-$ act as a sensitizer too, as its photolysis generates chlorine atoms whose reactivity towards hydrogen abstraction is surprisingly effective for synthesizing gold nanoparticles.[52]

Based on this finding, we immobilized H-donors on glass in order to grow gold nanoparticle monolayers. For this purpose, we tested the reactivity of two different homopolymers such as polystyrene (PS) and poly(2-vinylpyridine) (P2VP). Glass coverslips were coated with a thin polymer layer and a drop of a gold aqueous solution was flattened with a quartz coverslip (Fig. S1a†). Upon 4 min illumination with a low pressure UV lamp (dual emission at 254 nm – 20 W and 185 nm – 5 W), the substrates were characterized by scanning electron microscopy (SEM), which revealed the presence of randomly distributed gold nanoparticles of a few nanometres in diameter (Fig. S1b and c†). Although this procedure is rather effective without requiring any additional photosensitizers, it does not allow controlling neither nanoparticle organization nor morphology, necessary to tailor the optical properties of plasmonic substrates.

Micelle templated photochemistry to fabricate uniform arrays of gold potatoids

In order to simultaneously synthesize and organize gold nanoparticles on glass coverslips, we chose to work with amphiphilic polystyrene-*block*-poly(2-vinylpyridine) (PS-*b*-P2VP) as H-donor. In apolar solvents, PS-*b*-P2VP molecules form spherical micelles made of a PS shell and a P2VP core.[23] Micelles can play the role of nanocarriers by adding an acidic gold salt, which loads the micellar core with $[AuCl_4]^-$ by electrostatically interacting with protonated P2VP. Dip-coating a planar substrate into a micellar solution results in the uniform deposition and the assembly of gold-loaded micelles,[37] which will be used as reactive templates to fabricate plasmonic nanoparticles. Fig. 1 illustrates the evolution of the nanostructured substrate after each processing step by displaying schematics of the experimental setup and SEM images at different magnifications. Each series of images was taken with the InLens detector of the SEM for imaging the topography of micelles (Fig. S2a†) and the detector for secondary electrons (SE2) to picture the distribution of $[AuCl_4]^-$ or gold nanoparticles (Fig. 1a and c).[53] As gold anions are already present within the micelles, a water drop was flattened with a quartz coverslip on the ordered micellar monolayer to create a 10 μm thick layer between both interfaces. During this step, micelles undergo slight morphological changes and become sporadically sur-

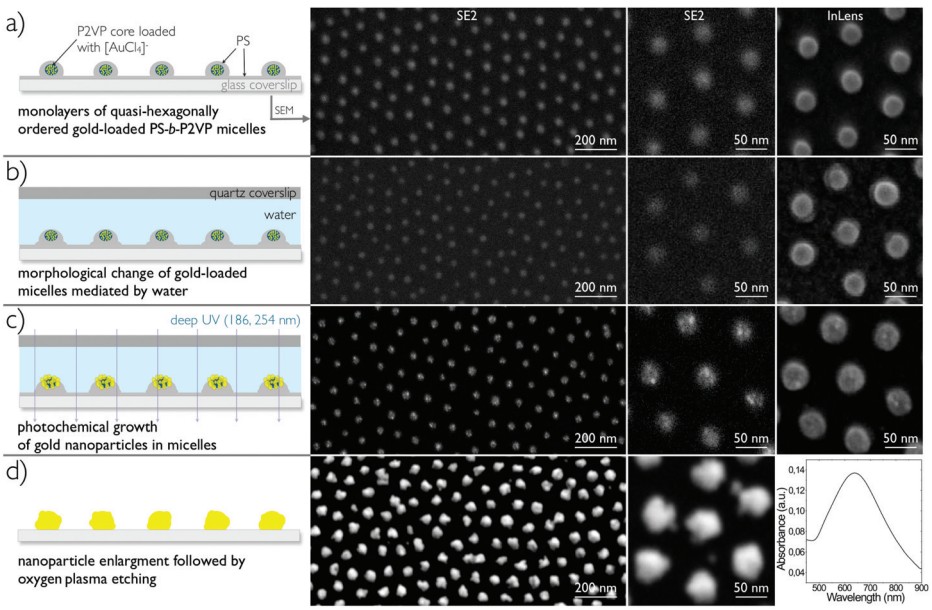

Fig. 1 Micellar photochemical lithography to fabricate randomly shaped gold potatoid arrays. Schematics and SEM images illustrating the evolution of the nanostructured substrate after each processing step: (a) upon dip coating, (b) flattening a water drop, (c) deep UV illumination and (d) electroless deposition followed by O_2 plasma etching. Each series of images was taken with the detector for secondary electrons (SE2) of the SEM to picture the distribution of $[AuCl_4]^-$ or gold nanoparticles, and with the InLens detector for imaging the topography of micelles, except for (d) where the extinction spectrum measured in air of the gold potatoid array is shown.

rounded by a polymer rim (Fig. 1b InLens). As the morphology of the gold-loaded P2VP cores does not change upon water exposure (Fig. 1b SE2), we suppose that a small structural rearrangement of the PS shell occurred due to its hydrophobic character. It was described that, without the presence of $[AuCl_4]^-$, PS-*b*-P2VP micellar films become porous upon exposure to polar solvents (Fig. S2b†). During this process, P2VP cores swell, break the upper side of the glassy PS shell and overflow outside the micelles to finally collapse upon drying the substrates.[54] In our case, micelle opening does not occur as $[AuCl_4]^-$ stabilizes the protonated P2VP cores. Next, we irradiated the immersed substrate with the UV lamp, which led to the formation of particles of a few nanometres exclusively localized at the micelle position (Fig. 1c). An irradiation time of 4 min was found to be sufficient to generate within individual micelles a few gold particles of about 8 nm in diameter and many gold seeds smaller than 3 nm (Fig. S3†). The preformed particles were then enlarged by electroless deposition (ED) by simply incubating the substrate in a gold aqueous solution in presence of a reducing agent. During ED, the nanoparticles originating from a same micelle increase in size and coalesce into a single particle (Fig. 2). Finally, the substrate was plasma cleaned to etch organic compounds away. With this protocol, we obtained quasi-hexagonally ordered arrays of deformed nanoparticles that we named "potatoids" (Fig. 1d). These arrays feature a nanoparticle interdistance of about 105 nm. With longer ED, the surface plasmon resonance of potatoids becomes more intense and red-shifted due to their larger size and non-spherical shape. Upon 10, 40 and 90 min of ED, potatoids have an average diameter of 38 ± 7, 51 ± 11 and 64 ± 12 nm with a plasmon band centred at 582, 614 and 623 nm, respectively, (Fig. 2 and S4a†).

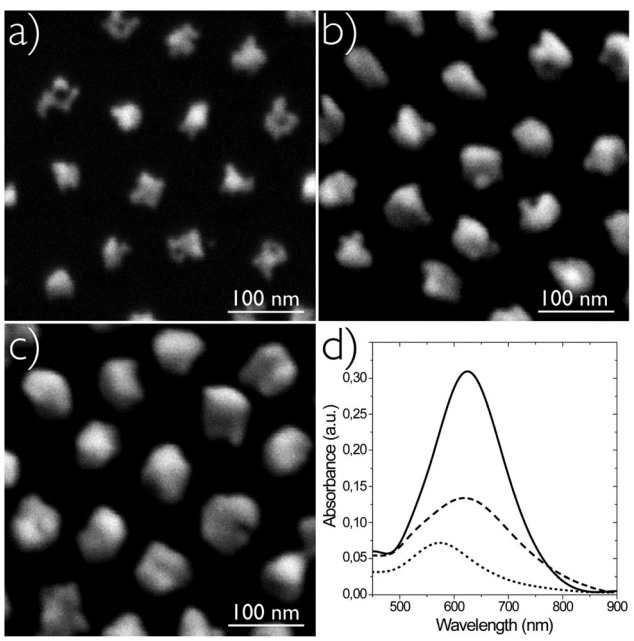

Fig. 2 Tuning the surface plasmon resonance of potatoid arrays with ED time. SEM images of potatoids grown for (a) 10, (b) 40 and (c) 90 min in a mixture of gold aqueous solution and ethanolamine. (d) Extinction spectra measured in air of gold potatoids grown for 10 (dots), 40 (dashes) and 90 min (line).

Photochemical nucleation of gold seeds in each micelle followed by particle enlargement constitutes a straightforward two-step approach for reproducibly introducing symmetry breaking in individual nanoparticles and tuning their surface plasmon resonance. For this purpose, it is important to enlarge gold seeds prior to plasma etching because inverting the step order leads to the formation of nanoparticle oligomers with a main absorbance at 540 nm (Fig. S4b and c†). Gold particles smaller than 3 nm are known to be thermodynamically less stable than larger ones,[55] thereby favouring particle melting and fusion during plasma treatment and then decreasing the number of gold seeds to be grown by ED.

Micropatterning gold potatoids

Photolithography is technologically essential in many applications. As it still requires sophisticated protocols based on the use of photosensitive coating called photoresists, high-throughput preparation of nanoparticle-coated substrates remains limited. In this context, we tested if micelle templated photochemistry was compatible with photoresist-free lithography. To this end, the quartz coverslip was replaced with a quartz photomask coated with a patterned chromium layer used to spatially block UV light and locally control gold growth. In doing so, uniform micropatterned structures of various geometries were successfully fabricated (Fig. 3). The quasi-hexagonal distribution and the irregular morphology of the gold nanoparticles were conserved (Fig. 3d). The smallest pattern size we obtained was about 500 nm (Fig. 3f), which makes this simple procedure more precise than most photoresist- and stamping-based approaches used to spatially control the micrometric distribution of nanoparticles over several centimeters.[42,56]

Gold nanorings and micelle opening

In an effort to further manipulate the shape of immobilized nanoparticles, we used a gold aqueous solution instead of water to improve the photochemical growth efficiency (Fig. 4a). Surprisingly, instead of generating more nanoparticles per micelle upon UV irradiation, we observed that gold growth occurred at the micelle periphery (Fig. 4b SE2) due to a structure reconstruction from spherical to pitted micelles (Fig. 4b InLens). During ED, gold seeds increase in size and fuse with each other to finally form ring-like structures. Upon plasma treatment, we obtained individual nanorings with an average outer diameter of 56 ± 4 nm and a wall thickness ranging from 9 to 15 nm (Fig. 4c). With this approach each nanoring displays a unique morphology with a structure that is not always fully looped while displaying wall thickness variations originating from the presence of larger seeds. Nevertheless, nanoring morphology and distribution are rather uniform (Fig. S6†) as such substrates feature a near-infrared absorbance centred at around 800 nm (Fig. 4c).

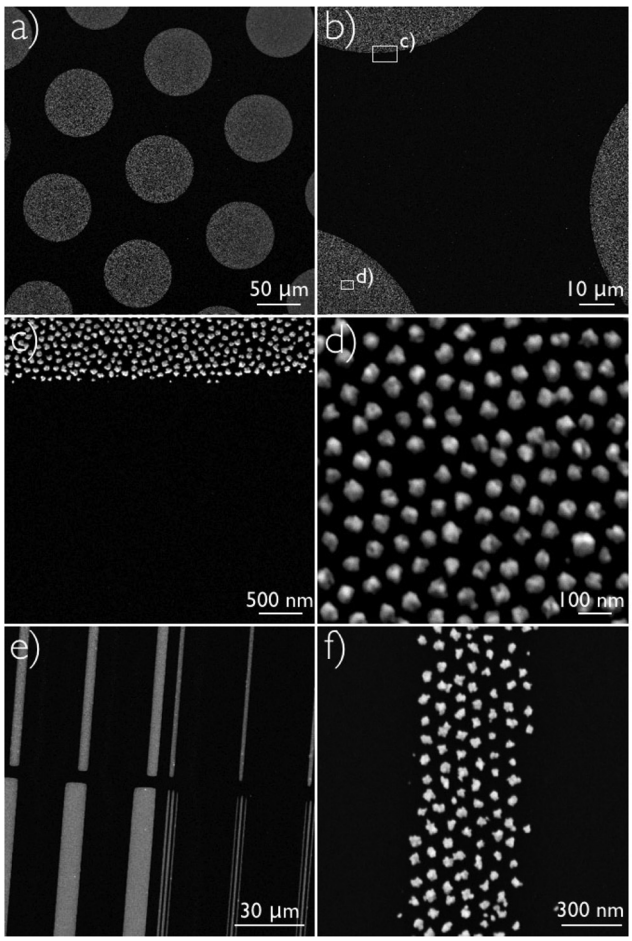

Fig. 3 Micelle templated photochemistry enables the micropatterning of gold potatoids. SEM images display various circular and linear micropatterns of gold potatoids at different magnifications. (c) and (d) Correspond to areas indicated in (b) and imaged at higher magnifications.

By increasing ED time, the absorbance of nanoring arrays becomes more intense but undergoes after 90 min a blue shift to 640 nm. This is due to the increase of the ring thickness ranging from 18 to 35 nm, which turns nanorings into structures with optical properties similar to the ones of randomly shaped nanoparticles (Fig. 5). The order of the two last proces-

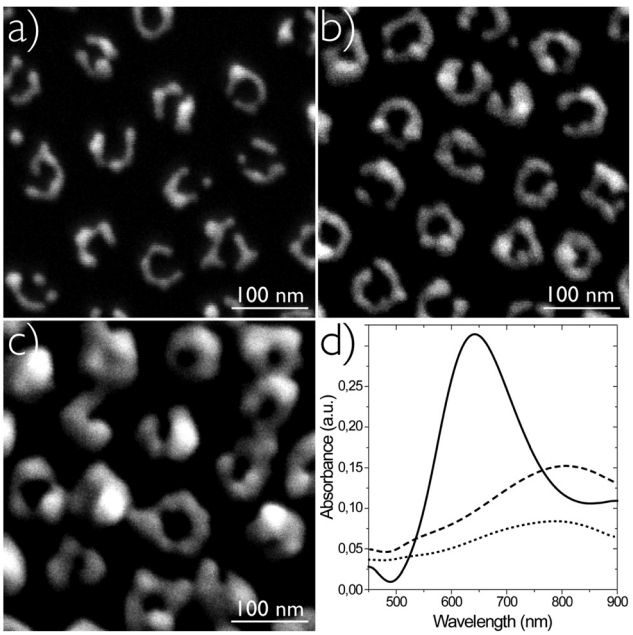

Fig. 5 Tuning the surface plasmon resonance of nanoring arrays with ED time. SEM images of nanorings grown for (a) 10, (b) 30 and (c) 90 min in a mixture of gold aqueous solution and ethanolamine. (d) Extinction spectra measured in air of gold nanorings grown for 10 (dots), 30 (dashes) and 90 min (line).

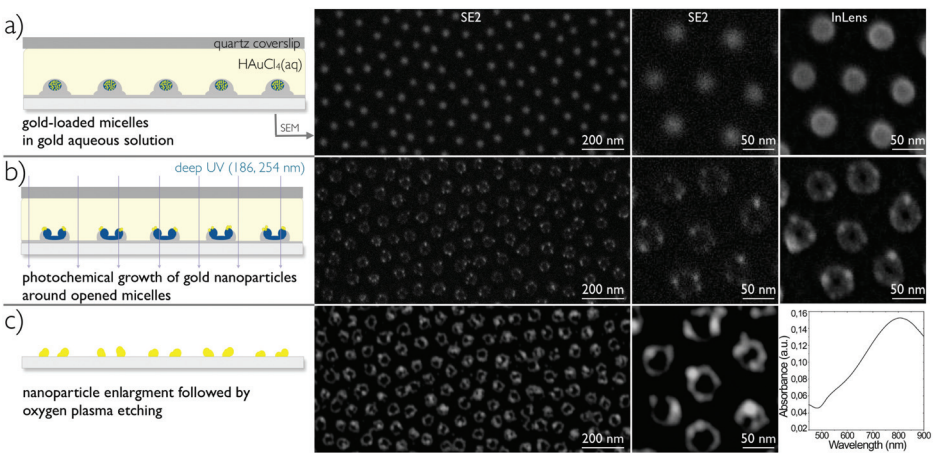

Fig. 4 Micellar photochemical lithography to fabricate gold nanoring arrays. Schematics and SEM images illustrating the evolution of the nanostructured substrate after each processing step: upon (a) flattening a drop of gold aqueous solution, (b) deep UV illumination and (c) electroless deposition followed by O_2 plasma etching. The extinction spectrum measured in air of the gold nanoring array is displayed in the lower right corner.

sing steps proved again to be critical for shaping gold nanoparticles as the inverted order leads to the circular assembly of individual dots and small aggregates mainly absorbing at 530 and 640 nm, respectively (Fig. S5a and b†).

To identify which experimental parameters mediate the structure reconstruction from spherical to pitted micelles, we tested our procedure while using monochromatic illumination (λ = 254 nm, 20 W). During the irradiation step, no morphological change was observed and gold growth occurred in 75% of micelles decorated with only one or two nanoparticles (Fig. S7†). Upon ED and plasma etching, arrays of spherical particles with a diameter of about 10 and 35 nm were obtained (Fig. S7b†). This observation indicates that 185 nm light efficiently mediates gold growth while partially oxidizing or etching the thin PS micellar shell,[38] so that P2VP chains are exposed to the liquid interface and partly shield PS to finally form pores.[54] Solubilized gold anions also play an active role in this process, as micelle opening did not take place upon irradiating micelles in water (Fig. 1). Unfortunately, we did not observe micelle opening upon micropatterning the substrate. By using a photomask, a sufficient UV dose may not be reached for triggering this process, thereby leading to the formation of potatoids (data not shown).

In comparison to other pore-making strategies for which one of the two polymer blocks is either etched away by physical means or reconstructed in presence of selective solvents,[57] our approach requires both mechanisms since the morphology of gold-loaded micelles is more difficult to manipulate than unloaded ones. Nevertheless, our strategy enables the fabrication of uniform nanoring arrays that feature a localized plasmon resonance in the near-infrared, whereas other BCML-based methods report the preparation of ring-like structures made of assembled nanoparticles, which were not optically characterized.[58–61]

Optical and photothermal properties of nanostructured gold rings and potatoids

Let us finally focus on the particular optical properties of the reported gold nanostructures and their relative benefits in comparison to plasmonic structures fabricated with physical methods. The main benefit we envision concerns their photothermal properties. We have already shown that arrays of spherical nanoparticles generated by BCML have proven to be valuable substrates in thermoplasmonics,[38,62–64] and assemblies of nanorings and potatoids make no exception. In nanoplasmonics, the incident light interacting with nanoparticles is scattered and/or absorbed, and the sum of these two processes is referred to as extinction. Among these three processes, absorption is the process of interest for applications in thermoplasmonics as it is the origin of the desired local temperature increase during illumination. To quantify the photothermal properties of the BCML substrates, we used the thermal microscopy imaging technique that we recently developed and named TIQSI (thermal imaging using quadriwave lateral shearing interferometry).[64] This technique enables the mapping of temperature and heat source density around gold nanoparticles lying upon a planar substrate (Fig. S8†). TIQSI also allows retrieving the absorption of the sample by integrating the heat source map and dividing the result by the incident laser power.[64] We performed such measurements for a set of wavelengths ranging from 711 nm to 864 nm (as permitted by our Ti-Sapphire laser) in order to reconstruct a quantitative absorption spectrum of the samples. In parallel, we performed quantitative extinction measurement in water by measuring the light intensity (I) crossing the substrate in two conditions: (I_1) with and (I_2) without gold nanoparticles. Extinction is then simply obtained using ext = $(I_2 - I_1)/I_2$. Finally, scattering can be quantified by subtracting extinction and absorption measurements.

As revealed by the measurements made in water, rings and potatoids feature a red-shifted surface plasmon resonance in comparison to the ones measured in air (Fig. 1d and 4c) and a great absorption-scattering ratio (Fig. 6a and d). Ring-like structures are even purely absorbing (Fig. 6a), *i.e.* negligible scattering occurs, and potatoids feature an absorption-scatter-

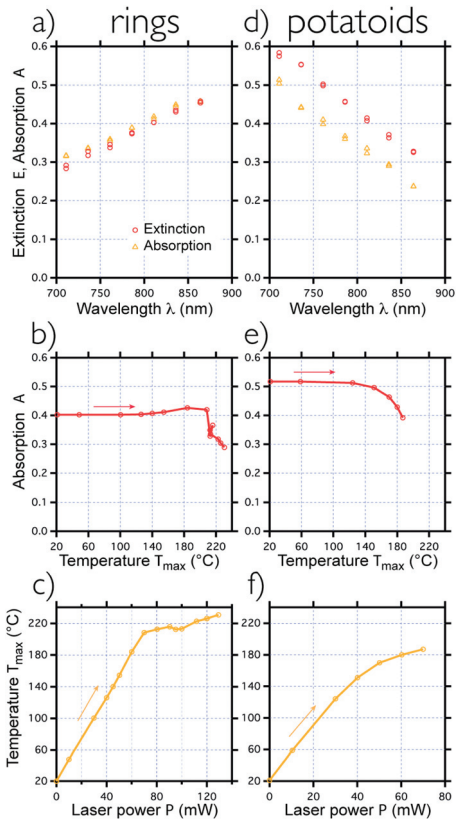

Fig. 6 Optical and photothermal properties of gold nanorings and potatoids in water. (a) Extinction and absorption of an array of nanorings (ED 30 min) as a function of the wavelength. (b) Absorption of an area of the nanorings measured after a 5-second laser exposure (λ = 786 nm), plotted as a function of the maximum temperature achieved during illumination. The arrow indicates the direction of the successive measurements. (c) Maximum temperature achieved as a function of the laser power. (d), (e) and (f) Correspond to the same series of measurements as (a), (b), and (c) for a potatoid nanoarray (ED 40 min, λ = 736 nm).

ing ratio of around 5 (Fig. 6d). This feature is rare in plasmonics in the near infrared, albeit beneficial for photothermal applications. For instance, plasmonic structures made by electron beam and colloidal lithography scatter a large fraction of the incident light due to their larger size, making them poor absorbers.[65]

We have recently shown that very high temperature increases can be achieved in aqueous solution far above the boiling point of the surrounding fluid at the vicinity of spherical gold nanoparticles synthesized by BCML (220 °C in water).[63] This phenomenon is termed superheating and occurs when no nucleation point for vapour bubble formation is present in the heated region. In this context, we have investigated the temperature sustainability of such substrates up to the temperature threshold for bubble formation (around 200 °C). In order to evidence any temperature-induced damage of the specimens, we measured the absorption of the samples subsequent to a 5-second illumination as a function of the temperature generated by the nanoparticle arrays. For these measurements, we considered the temperature at the centre of the illuminated area, *i.e.* the maximum temperature observed in the temperature maps (Fig. S8c†). Nanorings were stable up to around 200 °C (Fig. 6b and c), although a slight increase of the absorbance was observed from 130 °C, probably due a small change of the nanoparticle morphology. Potatoids were less stable as the absorbance tends to drop from 120 °C and the nanoparticles may detach from the substrate at around 190 °C as the absorbance decreases (Fig. 6e and f). In both cases, the reported gold structures are stable above the water boiling point and enable superheating. This observation means that nanorings and potatoids do not act as nucleation points. This conclusion opens the path for future applications involving near-infrared-induced thermal processes using potatoids and nanorings made by BCML.

Conclusions

We described a straightforward and cost-effective photochemical method to fabricate uniform arrays of gold nanoparticles on glass with micro/nanometric spatial resolution without requiring any additional photosensitizers or photoresists. By using block copolymer micellar monolayers as reactive templates, we fabricated plasmonic substrates with tuneable surface plasmon resonances. Depending on the extra-micellar chemical environment and the illumination wavelength, we succeeded in patterning and shaping optically active nanostructures such as gold potatoids and rings of about 50 nm in diameter that feature localized plasmon resonances above 600 and 800 nm, respectively. Quantification of their photothermal properties showed that nanoring-based substrates are temperature-resistant and features ideal photothermal properties, opening the path for future applications controlled by near-infrared light, including nanoscale solvothermal synthesis and spatiotemporal manipulation of biological systems within the tissue transparency window.

Acknowledgements

We thank R. Fässler for support. The Max Planck Society financially supported this work.

References

1 M. Daniel and D. Astruc, *Chem. Rev.*, 2004, **104**, 293–346.
2 P. K. Jain, K. S. Lee, I. H. El-Sayed and M. A. El-Sayed, *J. Phys. Chem. B*, 2006, **110**, 7238–7248.
3 S. E. Lohse and C. J. Murphy, *Chem. Mater.*, 2013, **25**, 1250–1261.
4 N. J. Halas, S. Lal, W.-S. Chang, S. Link and P. Nordlander, *Chem. Rev.*, 2011, **111**, 3913–3961.
5 M. A. Mahmoud, D. O'Neil and M. A. El-Sayed, *Chem. Mater.*, 2014, **26**, 44–58.
6 Y. Jin, *Adv. Mater.*, 2012, **24**, 5153–5165.
7 B. Yan, S. V. Boriskina and B. M. Reinhard, *J. Phys. Chem. C*, 2011, **115**, 24437–24453.
8 G. Baffou and R. Quidant, *Laser Photon. Rev.*, 2013, **7**, 171–187.
9 E. Boulais, R. Lachaine, A. Hatef and M. Meunier, *J. Photochem. Photobiol., C*, 2013, **17**, 26–49.
10 R. Near, C. Tabor, J. Duan, R. Pachter and M. El-Sayed, *Nano Lett.*, 2012, **12**, 2158–2164.
11 G. Zhang and D. Wang, *Chem. – Asian J.*, 2009, **4**, 236–245.
12 Y. Li, W. Cai and G. Duan, *Chem. Mater.*, 2008, **20**, 615–624.
13 S. Ullrich, S. P. Scheeler, C. Pacholski, J. P. Spatz and S. Kudera, *Part Part. Syst. Charact.*, 2012, **30**, 102–108.
14 M. B. Müller, C. Kuttner, T. A. F. König, V. V. Tsukruk, S. Förster, M. Karg and A. Fery, *ACS Nano*, 2014, **8**, 9410–9421.
15 L. Wang, F. Montagne, P. Hoffmann, H. Heinzelmann and R. Pugin, *J. Colloid Interface Sci.*, 2011, **356**, 496–504.
16 C. Farcau, N. M. Sangeetha, N. Decorde, S. Astilean and L. Ressier, *Nanoscale*, 2012, **4**, 7870.
17 J. Fontana, J. Livenere, F. J. Bezares, J. D. Caldwell, R. Rendell and B. R. Ratna, *Appl. Phys. Lett.*, 2013, **102**, 201606.
18 W. Lee, S. Y. Lee, R. M. Briber and O. Rabin, *Adv. Funct. Mater.*, 2011, **21**, 3424–3429.
19 L. Vigderman, B. P. Khanal and E. R. Zubarev, *Adv. Mater.*, 2012, **24**, 4811–4841.
20 M. Mueller, M. Tebbe, D. V. Andreeva, M. Karg, R. A. Alvarez-Puebla, N. Pazos Perez and A. Fery, *Langmuir*, 2012, **28**, 9168–9173.
21 M. Park, C. Harrison, P. Chaikin, R. Register and D. Adamson, *Science*, 1997, **276**, 1401–1404.
22 S. B. Darling, *Prog. Polym. Sci.*, 2007, **32**, 1152–1204.
23 S. Forster, *Top. Curr. Chem.*, 2003, **226**, 1–28.
24 C. Brinker, Y. Lu, A. Sellinger and H. Fan, *Adv. Mater.*, 1999, **11**, 579.
25 F. L. Yap, P. Thoniyot, S. Krishnan and S. Krishnamoorthy, *ACS Nano*, 2012, **6**, 2056–2070.

26 W. J. Cho, Y. Kim and J. K. Kim, *ACS Nano*, 2012, **6**, 249–255.
27 W. Lopes and H. Jaeger, *Nature*, 2001, **414**, 735–738.
28 J. Y. Cheng, C. A. Ross, V. Chan, E. L. Thomas, R. Lammertink and G. J. Vancso, *Adv. Mater.*, 2001, **13**, 1174.
29 I. Vukovic, G. ten Brinke and K. Loos, *Polymer*, 2013, **54**, 2591–2605.
30 T. Thurn-Albrecht, J. Schotter, C. A. Kastle, N. Emley, T. Shibauchi, L. Krusin-Elbaum, K. Guarini, C. T. Black, M. T. Tuominen and T. P. Russell, *Science*, 2000, **290**, 2126–2129.
31 H.-S. Moon, J. Y. Kim, H. M. Jin, W. J. Lee, H. J. Choi, J. H. Mun, Y. J. Choi, S. K. Cha, S. H. Kwon and S. O. Kim, *Adv. Funct. Mater.*, 2014, **24**, 4343–4348.
32 Y. Wang, M. Becker, L. Wang, J. Liu, R. Scholz, J. Peng, U. Gösele, S. Christiansen, D. H. Kim and M. Steinhart, *Nano Lett.*, 2009, **9**, 2384–2389.
33 M. Aizawa and J. M. Buriak, *Chem. Mater.*, 2007, **19**, 5090–5101.
34 L. A. Porter, H. C. Choi, J. M. Schmeltzer, A. E. Ribbe, L. C. C. Elliott and J. M. Buriak, *Nano Lett.*, 2002, **2**, 1369–1372.
35 T. Brezesinski, M. Groenewolt, A. Gibaud, N. Pinna, M. Antonietti and B. M. Smarsly, *Adv. Mater.*, 2006, **18**, 2260.
36 J. Polleux, M. Rasp, I. Louban, N. Plath, A. Feldhoff and J. P. Spatz, *ACS Nano*, 2011, **5**, 6355–6364.
37 G. Kastle, H. Boyen, F. Weigl, G. Lengl, T. Herzog, P. Ziemann, S. Riethmuller, O. Mayer, C. Hartmann, J. Spatz, M. Moller, M. Ozawa, F. Banhart, M. Garnier and P. Oelhafen, *Adv. Funct. Mater.*, 2003, **13**, 853–861.
38 M. Zhu, G. Baffou, N. Meyerbröker and J. Polleux, *ACS Nano*, 2012, **6**(8), 7227–7233.
39 J. Chai, D. Wang, X. Fan and J. M. Buriak, *Nat. Nanotechnol.*, 2007, **2**, 500–506.
40 J. Chai and J. M. Buriak, *ACS Nano*, 2008, **2**, 489–501.
41 Y. Liu, K. Yehl, Y. Narui and K. Salaita, *J. Am. Chem. Soc.*, 2013, **135**, 5320–5323.
42 T. Lohmueller, D. Aydin, M. Schwieder, C. Morhard, I. Louban, C. Pacholski and J. P. Spatz, *Biointerphases*, 2011, **6**, MR1–MR12.
43 N. G. Caculitan, H. Kai, E. Y. Liu, N. Fay, Y. Yu, T. Lohmüller, G. P. O'Donoghue and J. T. Groves, *Nano Lett.*, 2014, **14**, 2293–2298.
44 A. J. Mieszawska, G. W. Slawinski and F. P. Zamborini, *J. Am. Chem. Soc.*, 2006, **128**, 5622–5623.
45 A. J. Mieszawska and F. P. Zamborini, *Chem. Mater.*, 2005, **17**, 3415–3420.
46 S. Kumar, H. Yang and S. Zou, *J. Phys. Chem. C*, 2007, **111**, 12933–12938.
47 N. Taub, O. Krichevski and G. Markovich, *J. Phys. Chem. B*, 2003, **107**, 11579–11582.
48 L. Osinkina, T. Lohmüller, F. Jäckel and J. Feldmann, *J. Phys. Chem. C*, 2013, **117**, 22198–22202.
49 M. Sakamoto, M. Fujistuka and T. Majima, *J. Photochem. Photobiol., C*, 2009, **10**, 33–56.
50 J. C. Scaiano, K. G. Stamplecoskie and G. L. Hallett-Tapley, *Chem. Commun.*, 2012, **48**, 4798.
51 S. Eustis and M. A. El-Sayed, *J. Phys. Chem. B*, 2006, **110**, 14014–14019.
52 K. L. McGilvray, J. Granger, M. Correia, J. T. Banks and J. C. Scaiano, *Phys. Chem. Chem. Phys.*, 2011, **13**, 11914.
53 V. Kochat, A. N. Pal, E. S. Sneha, A. Sampathkumar, A. Gairola, S. A. Shivashankar, S. Raghavan and A. Ghosh, *J. Appl. Phys.*, 2011, 110.
54 Z. Chen, C. He, F. Li, L. Tong, X. Liao and Y. Wang, *Langmuir*, 2010, **26**, 8869–8874.
55 K. Koga, T. Ikeshoji and K.-I. Sugawara, *Phys. Rev. Lett.*, 2004, **92**, 115507.
56 J. Chen, P. Mela, M. Moeller and M. C. Lensen, *ACS Nano*, 2009, **3**, 1451–1456.
57 Y. Wang and F. Li, *Adv. Mater.*, 2011, **23**, 2134–2148.
58 L. Wang, F. Montagne, P. Hoffmann and R. Pugin, *Chem. Commun.*, 2009, 3798.
59 X. Zu, X. Hu, L. A. Lyon and Y. Deng, *Chem. Commun.*, 2010, **46**, 7927.
60 J.-H. Ryu, S. Park, B. Kim, A. Klaikherd, T. P. Russell and S. Thayumanavan, *J. Am. Chem. Soc.*, 2009, **131**, 9870–9871.
61 H. Cho, S. Choi, J. Y. Kim and S. Park, *Nanoscale*, 2011, **3**, 5007.
62 G. Baffou, P. Berto, E. Bermúdez Ureña, R. Quidant, S. Monneret, J. Polleux and H. Rigneault, *ACS Nano*, 2013, **7**, 6478–6488.
63 G. Baffou, J. Polleux, H. Rigneault and S. Monneret, *J. Phys. Chem. C*, 2014, **118**, 4890–4898.
64 G. Baffou, P. Bon, J. Savatier, J. Polleux, M. Zhu, M. Merlin, H. Rigneault and S. Monneret, *ACS Nano*, 2012, **6**, 2452–2458.
65 H.-Y. Tseng, W.-F. Chen, C.-K. Chu, W.-Y. Chang, Y. Kuo, Y.-W. Kiang and C. C. Yang, *Nanotechnology*, 2013, **24**, 065102.

Nanoscale

Supporting Information

Shaping and Patterning Gold Nanoparticles *via* Micelle Templated Photochemistry

F. Kundrat,[a] G. Baffou[b] and J. Polleux*[a,c]

[a] *Max Planck Institute of Biochemistry, Department of Molecular Medicine, 82152 Martinsried, Germany.*
[b] *Fresnel Institute UMR 7249, CNRS, Aix-Marseille Université, Ecole Centrale Marseille, 13013 Marseille, France.*
[c] *Center for NanoScience, Ludwig Maximilian University, 80799 Munich, Germany.*

†Electronic Supplementary Information (ESI) available: Additional SEM, TEM and extinction measurements further describe the mechanism of the reported photochemical approach. See DOI: 10.1039/x0xx00000x

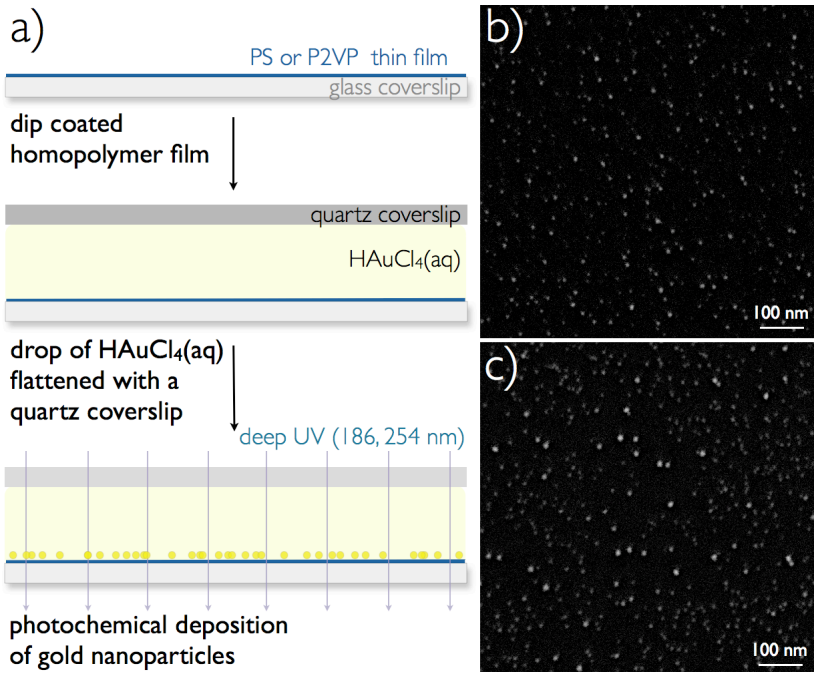

Figure S1. Photochemical deposition of gold nanoparticle monolayers on homopolymer thin films. a) Schematics describing the experimental procedure necessary to fabricate plasmonic substrates. SEM images displaying gold nanoparticles supported on b) PS- and c) P2VP-coated glass after 4-min deep UV irradiation.

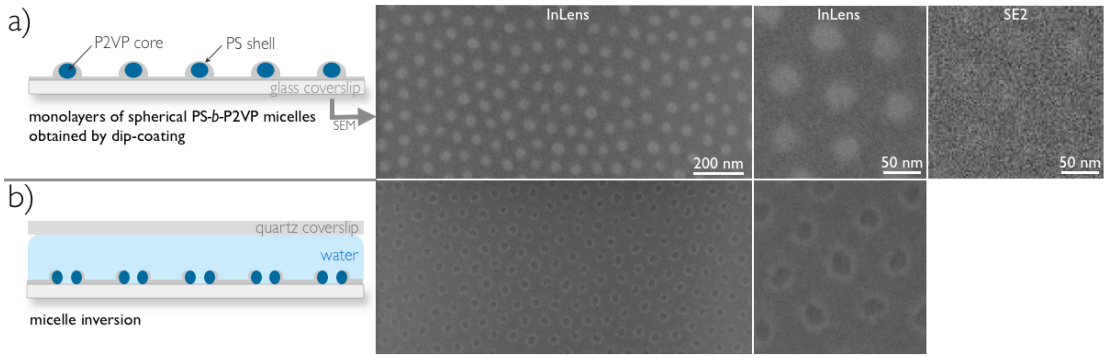

Figure S2. Water-mediated micelle opening. Schematics and SEM images illustrating the evolution of unloaded PS-*b*-P2VP micelles a) before and b) after morphology reconstruction induced by their immersion in water for 4 min. These images display a quasi-hexagonally ordered micellar monolayer, which becomes porous due to water-mediated swelling of the P2VP block, thereby rupturing the PS shell to finally form ring-like structures.

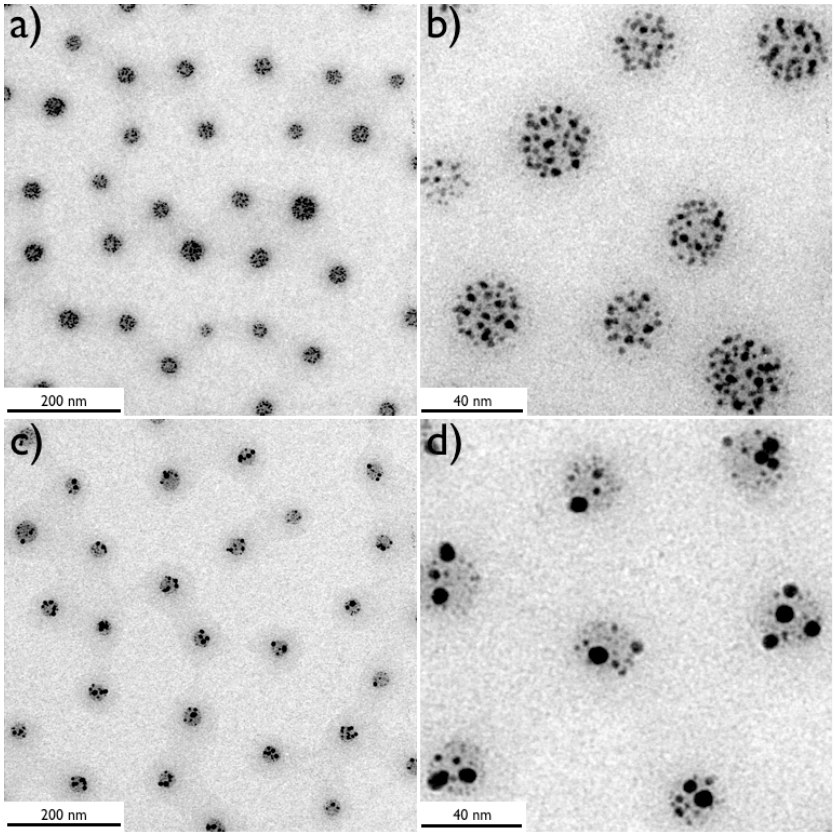

Figure S3. Photochemical growth of gold nanoparticles within micelles. Transmission electron microscopy (TEM) of gold-loaded micelles deposited on a copper grid coated with a SiO_2 film a),b) before and c),d) after deep UV illumination for 4 min in water.

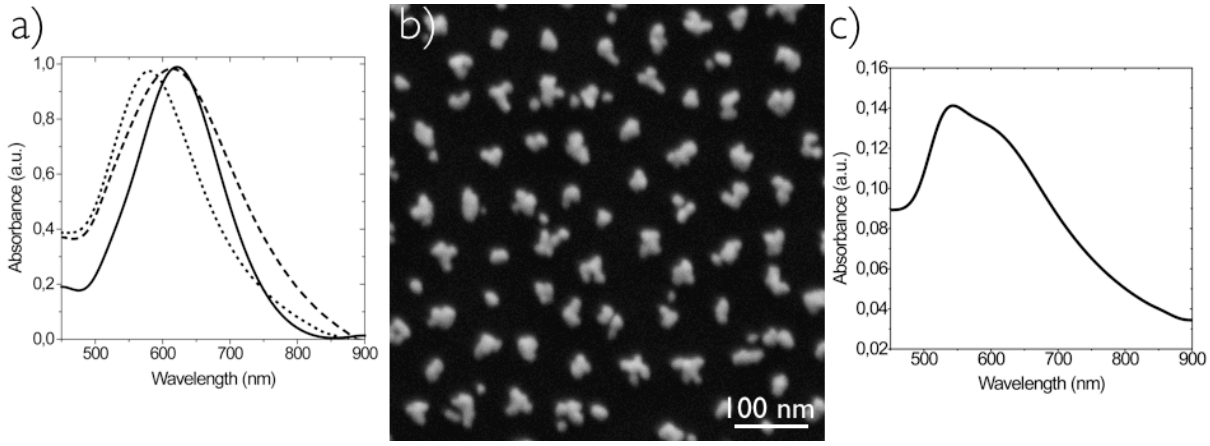

Figure S4. a) Normalized extinction spectra of gold potatoids grown for 10 (dots), 40 (dashes) and 90 min (line) in a mixture of gold aqueous solution and ethanolamine. b) SEM images displaying gold nanostructures prepared upon inverting the two last processing steps in comparison to the protocol described in Figure 1. c) Extinction spectrum of the gold nanostructures displayed in b).

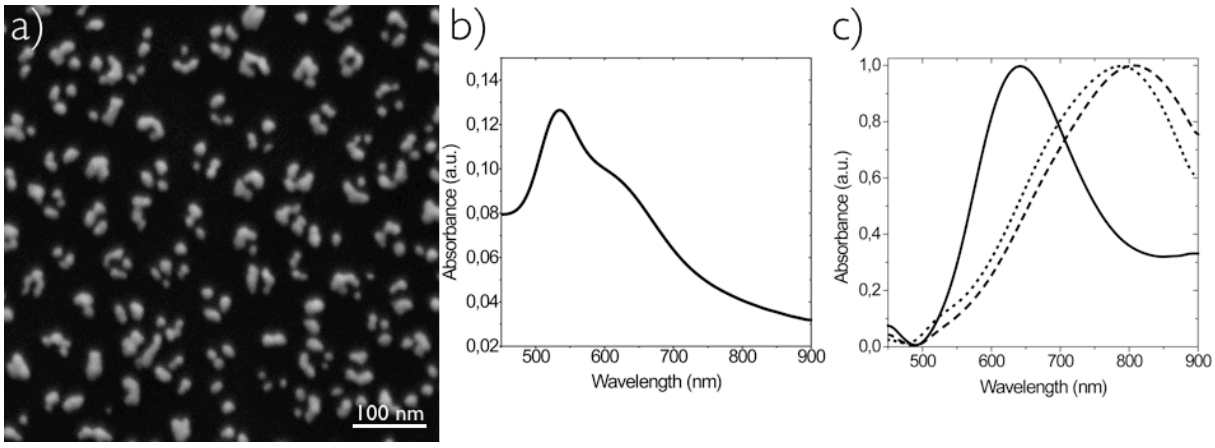

Figure S5. a) SEM images displaying gold nanostructures prepared upon inverting the two last processing steps in comparison to the protocol described in Figure 4. b) Extinction spectrum of the gold nanostructures displayed in a). c) Normalized extinction spectra of gold nanorings grown for 10 (dots), 30 (dashes) and 90 min (line) in a mixture of gold aqueous solution and ethanolamine.

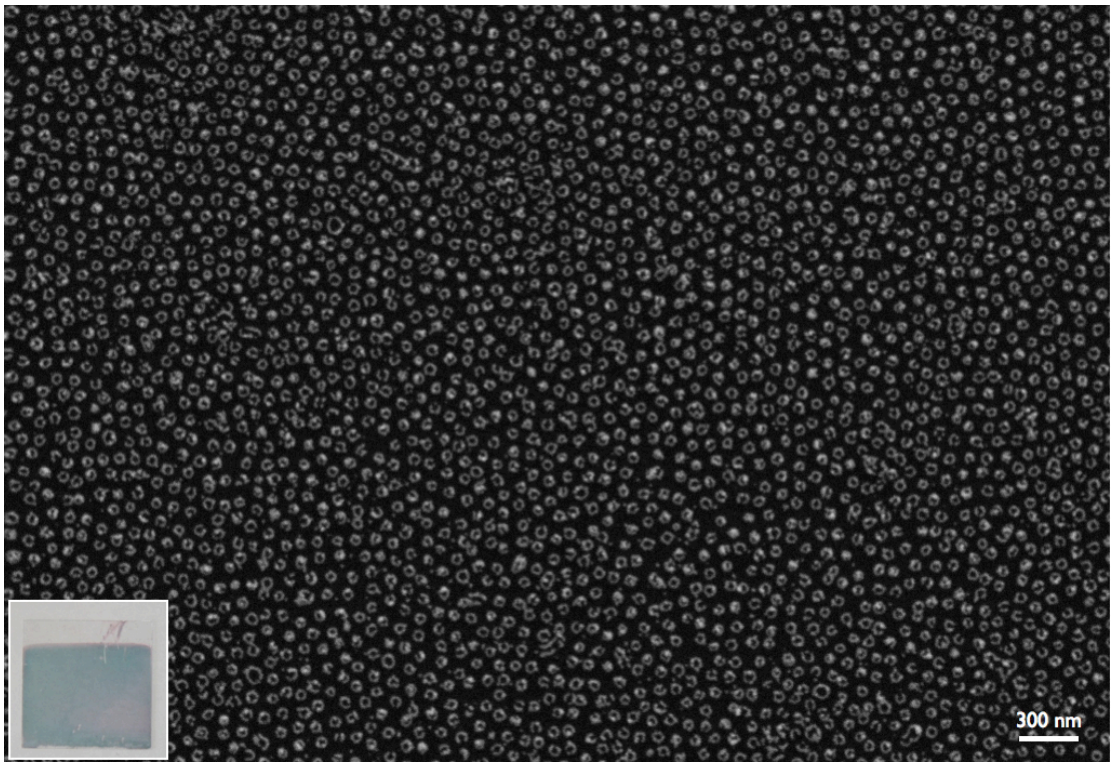

Figure S6. SEM image showing an overview of a uniform gold nanoring array. Inset displays an 18x18 mm glass coverslip coated with the nanoring array.

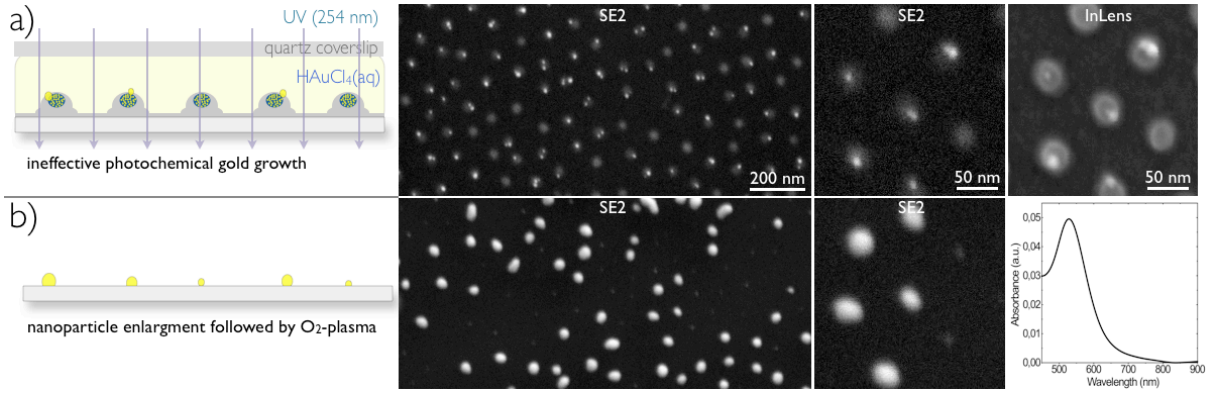

Figure S7. Monochromatic illumination (λ = 254 nm) does not enable the fabrication of gold nanoring arrays. Schematics and SEM images illustrating the evolution of the nanostructured substrate upon a) deep UV illumination and b) electroless deposition followed by O_2 plasma etching. The extinction spectrum of the gold nanoarrays is shown in b).

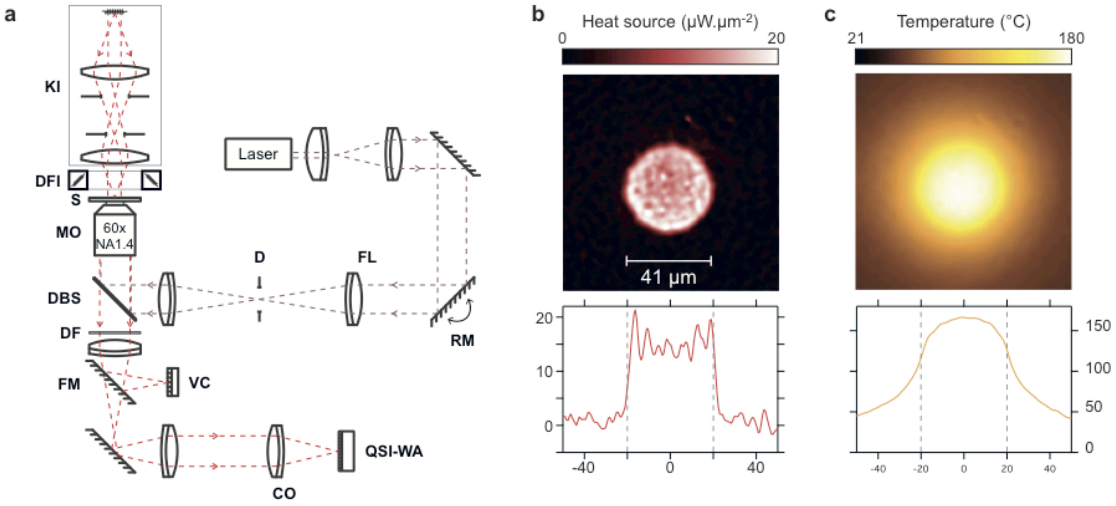

Figure S8. a) Schematic of the optical setup used for thermal microscopy measurements. KI: Köhler illumination, DFI: Dark Field Imaging. S: Sample, DBS: Dichroic Beam Splitter, DF: Dichroic Filter, FM: flip mirror, VC: Video Camera, CO: Camera Objective, QSI-WA: Wavefront analyzer based on Quadriwave Shearing Interferometry. D: Diaphragm, FL: Flip Lens, RM: Rotating Mirror. b) Map of the heat source density. c) Map of the temperature distribution. Figures b) and c) correspond to the same measurement of a laser beam (41 µm in diameter, lambda=736 nm, 63 mW) impinging on a potatoid substrate.

7.2. Manuscript II

Light-Assisted Solvothermal Chemistry Using Plasmonic Nanoparticles

I contributed to this study by providing gold nanoring arrays that I prepared based on the method developed in Manuscript I. Furthermore, I contributed to figures and writing.

Published as:
Robert H, **Kundrat F**, Bermúdez-Ureña E, Rigneault H, Monneret S, Quidant R, Polleux J, Baffou G. Light-Assisted Solvothermal Chemistry Using Plasmonic Nanoparticles. *ACS Omega*, 2016 (1), 2–8.

ACS OMEGA

Article

http://pubs.acs.org/journal/acsodf

Light-Assisted Solvothermal Chemistry Using Plasmonic Nanoparticles

Hadrien M. L. Robert,[*,†,‡] Franziska Kundrat,[¶] Esteban Bermúdez-Ureña,[§] Hervé Rigneault,[†] Serge Monneret,[†] Romain Quidant,[§,∥] Julien Polleux,[¶,#] and Guillaume Baffou[*,†]

[†]Institut Fresnel, CNRS, Aix-Marseille Université, Centrale Marseille, UMR 7249, 13013 Marseille, France

[‡]PHASICS S.A., Parc technologique de Saint Aubin, Route de l'Orme des Merisiers, 91190 Saint Aubin, France

[¶]Department of Molecular Medicine, Max Planck Institute of Biochemistry, 82152 Martinsried, München, Germany

[§]ICFO - Institut de Ciències Fotòniques, The Barcelona Institute of Science and Technology, 08860 Castelldefels, Barcelona, Spain

[∥]ICREA - Institució Catalana de Recerca i Estudis Avançats, 08010 Barcelona, Spain

[#]Center for NanoScience, Ludwig Maximilian University, 80799 Munich, Germany

ABSTRACT: Solvothermal synthesis, denoting chemical reactions occurring in metastable liquids above their boiling point, normally requires the use of a sealed autoclave under pressure to prevent the solvent from boiling. This work introduces an experimental approach that enables solvothermal synthesis at ambient pressure in an open reaction medium. The approach is based on the use of gold nanoparticles deposited on a glass substrate and acting as photothermal sources. To illustrate the approach, the selected hydrothermal reaction involves the formation of indium hydroxide microcrystals favored at 200 °C in liquid water. In addition to demonstrating the principle, the benefits and the specific characteristics of such an approach are investigated, in particular, the much faster reaction rate, the achievable spatial and time scales, the effect of microscale temperature gradients, the effect of the size of the heated area, and the effect of thermal-induced microscale fluid convection. This technique is general and could be used to spatially control the deposition of virtually any material for which a solvothermal synthesis exists.

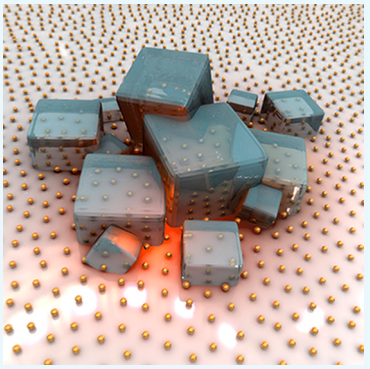

INTRODUCTION

Plasmon-induced nanochemistry (PINC) is an active area of research that benefits from the plasmonic properties of metal nanoparticles to enhance or enable chemical reactions on small scales.[1] Three main features of plasmonic nanoparticles have been involved so far in PINC: (1) the enhanced optical near field of nanoparticles,[2−4] which favors photochemical reactions in the vicinity of the illuminated particles, (2) heat generation,[5−10] which favors local chemical synthesis according to the Arrhenius law, and (3) hot electron/hole injection,[11−13] a recently proposed mechanism leading to localized redox reactions. These multiple facets of plasmonic nanoparticles provide a wide variety of tools to develop new applications in nanochemistry. The aim of this work is to introduce a novel approach in PINC based on the use of plasmonic nanoparticles as nanosources of heat, enabling solvothermal reactions.

Solvothermal chemical synthesis relies on the use of superheated liquid solvents, that is, liquids heated above their boiling point. For water, it typically corresponds to temperature ranging from 100 to 380 °C. To prevent the solvent from boiling and to keep it a liquid at such high temperatures, the standard procedure involves the use of a sealed chamber, named an *autoclave*, in which the temperature increase concomitantly creates a pressure increase that maintains the solvent in a liquid state.

The interest of a solvothermal (or hydrothermal) synthesis is manifold. For instance, many organic compounds that are inert in liquid water become reactive when the temperature is increased far above 100 °C, especially reactions that occur only in the presence of strong acid or base. Indeed, as temperature increases from 20 to 300 °C, the ionic product of water increases by three orders of magnitude, from $10^{-14.0}$ to $10^{-11.3}$. The resulting higher concentrations of OH^- and H_3O^+ simultaneously increase the rate of both acid- and base-catalyzed reactions in liquid water far beyond the natural acceleration thermally governed by the Arrhenius law. Moreover, the dielectric constant of water decreases from 80.1 down to 19.7 over this range of temperature, which results in a strong decrease of the polarity of water molecules and in a natural rise of solubility of ionic compounds. Today, the growing interest in using hydrothermal synthesis derives from its advantages in terms of high reactivity of reactants, formation of a metastable and unique solvent, and low energy consumption.[14] The main constraint of such an approach relies on the use of an autoclave, which prevents any chemical exchange and monitoring during the reaction.

Received: April 20, 2016
Accepted: May 6, 2016
Published: July 6, 2016

DOI: 10.1021/acsomega.6b00019
ACS Omega 2016, 1, 2−8

In this article, we show that solvothermal synthesis can be achieved under ambient conditions without requiring a pressure chamber when heating is performed by illuminating a substrate patterned with metal nanoparticles illuminated at their plasmonic resonance. Such experimental conditions prevent the liquid from boiling, up to around 220 °C, as recently evidenced in a previous work.[15] We illustrate this approach with a well-established solvothermal chemical reaction involving the synthesis of indium hydroxide microcrystals in water. After describing the experimental conditions and the results, we dedicate a final part to discuss the interest, the benefits and the limitations of plasmon-assisted solvothermal chemistry (PASC).

RESULTS

Liquid Superheating Using Metal Nanoparticles. Under illumination at their plasmonic resonance wavelength, metal nanoparticles can turn into efficient heat sources. This effect is the basis of an active field of research named thermoplasmonics,[16] involving promising biomedical applications. We have recently shown that, against all odds, water superheating can be achieved at ambient pressure by heating plasmonic nanoparticles on a glass substrate using continuous wave (cw) laser illumination.[15] The geometry of the system is depicted in Figures 1 and 2. The sample was composed of a glass coverslip patterned with (1) a uniform distribution of gold nanorings made by block copolymer micellar lithography (BCML)[17] (see Figure 1a) or (2) isolated gold disks, 500 nm in diameter and 40 nm thick, made by e-beam lithography (EBL) (not shown).

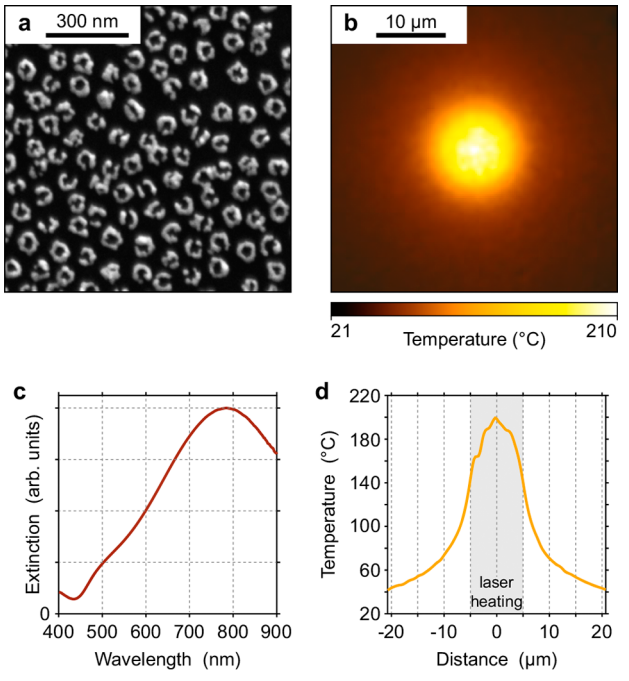

Figure 1. (a) Gold nanorings on a glass substrate made by BCML. (b) Associated temperature distribution (155 × 155 px) when the sample is illuminated with a laser beam, 10 μm in diameter, reaching a value close to 200 °C at the center of the heated area. (c) Extinction spectrum of the BCML substrate made of gold nanorings in water. (d) Temperature profile related to image (b) averaged over 11 successive horizontal lines across the center of the image.

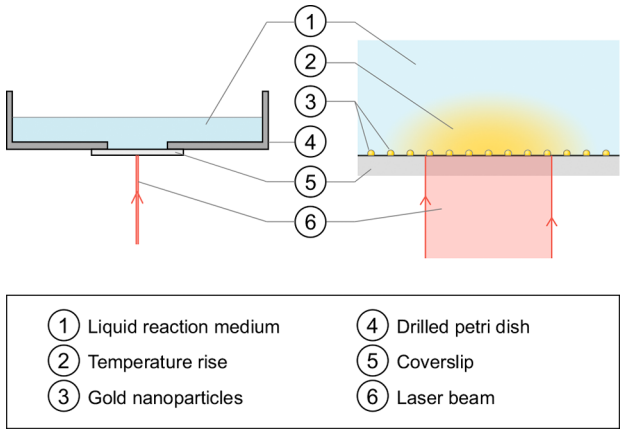

Figure 2. Side view of the sample where the hydrothermal synthesis takes place.

The coverslip was pasted on the back of a drilled Petri dish, which was filled with the reactants freshly dissolved in deionized (Milli-Q) water (Figure 2). The sample was finally placed on an optical microscope enabling optical (intensity and phase) imaging, laser heating and temperature imaging at the submicrometric scale (see ref 18 for details). Heating was performed by illuminating the sample from below (i.e., from the glass side) using a laser beam at λ = 800 nm, matching the plasmonic resonance wavelength of the gold nanoparticles. When working with BCML samples, the beam profile at the glass/water interface was expanded to obtain a uniform (not Gaussian) beam with a diameter that could be adjusted from a few microns to a few hundreds of microns using an iris (see Figure 1b). When working with EBL samples, the laser beam was rather focused on a single gold disk using a 100× objective, NA 1.3. In any configuration, water superheating was systematically observed but we have never seen water boiling at 100 °C. Bubble formation systematically occurred around 220 ± 10 °C, as evidenced experimentally by the thermal microscopy technique we developed (Figure 1b).[18]

The reason why water does not boil is that this system is free from nucleation points, such as scratches, micrometric cavities, impurities, and so on. Glass surfaces are particularly flat by nature, and it turns out that gold nanoparticles do not act as nucleation point themselves.[15]

Hydrothermal Synthesis. Hydrothermal synthesis refers to solvothermal synthesis where the solvent is water. To simply evidence that solvothermal synthesis can be conducted at ambient pressure using gold nanoparticles, we selected a hydrothermal chemical reaction[19] that involves the formation of solid particles, namely, the chemical transformation of indium chloride to indium hydroxide crystals

$$InCl_{3(aq)} + 3OH^- \xrightarrow{200\ °C} In(OH)_{3(s)} + 3Cl^-$$

Typical crystals obtained with this approach feature a cubic crystallographic symmetry, as evidenced in ref 19.

We initially prepared a solution under the same experimental conditions as in ref 19. We dissolved 0.21 g of $InCl_3$, 9.4 mg of NaOH, and 12.5 μL of NH_3 in 24 mL of water, which gave a concentration of c_m = 40 mM $InCl_3$. This solution was then diluted 10, 100, or 1000 times before being added into the Petri dish. Prior to each experiment, calibration was made using our thermal microscopy technique with pure water in the sample to determine which laser power was required to reach 200 °C for a

DOI: 10.1021/acsomega.6b00019
ACS Omega 2016, 1, 2−8

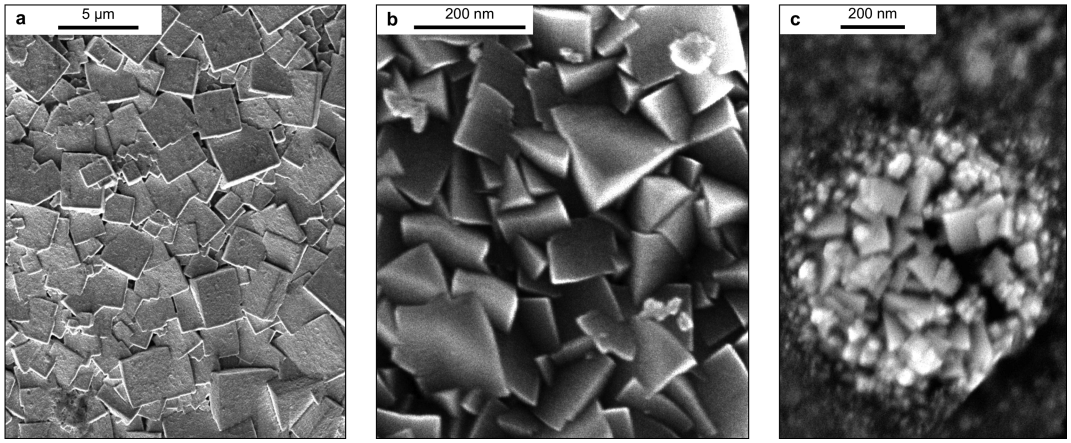

Figure 3. Effect of the size of the heated area. (a) SEM image of $In(OH)_3$ microcrystals formed upon heating an area of 500 μm in diameter (BCML sample, laser exposure time δt = 1 h, laser power = 380 mW, maximum temperature T_0 = 200 °C, and reactant concentration c_m = 40 mM). (b) SEM image of $In(OH)_3$ microcrystals formed upon heating an area of 10 μm in diameter (BCML sample, laser exposure time δt = 1 h, laser power = 18.5 mW, maximum temperature T_0 = 200 °C, and reactant concentration $c_0 = c_m/10$ = 4 mM). (c) SEM image of $In(OH)_3$ microcrystals formed upon heating a single gold disk, 430 nm in diameter (EBL sample, laser exposure time δt = 10 min, laser power = 0.43 mW, maximum temperature T_0 = 200 °C, and reactant concentration $c_0 = c_m/1000$ = 0.04 mM).

given laser beam size. Note that the use of a thermal microscopy technique is not mandatory; if a setup is not endowed with a means of temperature characterization, it is possible to ensure a temperature of around 200 °C by setting the laser power slightly below the laser power threshold for bubble formation (supposed to be around 230 °C).

In our approach, a set of four parameters can be adjusted, namely, (1) the laser beam diameter D (i.e., the size of the heated area in the case of BCML samples), (2) the temperature T_0 (taken at the center of the heated area), (3) the initial reactant concentration c_0, and (4) the heating duration δt.

Reaction Kinetics. We first conducted experiments upon heating at T_0 = 200 °C an area with a diameter ranging from 430 nm (gold disk) to 500 μm (BCML sample). Figure 3 shows SEM (scanning electron microscopy) images taken at the center of the illuminated area where cubic $In(OH)_3$ crystals have grown. Several important observations can be made.

(1) In comparison with the standard high-pressure procedure, which yields the formation of isolated clusters of particles, the local photothermal approach leads to a dense coverage of the substrate where the crystals can be partially merged with each other. The dimension of the crystals ranged from a few 100 nm to 4 μm, which is comparable with common results obtained with an autoclave.

(2) The smaller the heated area, the faster the reaction rate. For instance, when using a single gold disk, 430 nm in diameter, we observed a fast crystal formation (10 min) although the reactant concentration was divided by a factor of 1000 ($c_0 = c_m/1000$). We interpret this observation by the constant renewal of the reactants in the confined heated volume because of Brownian motion, fluid convection,[20] and thermophoresis.[21−23] Indeed, the micrometric reaction volume is in contact with a quasi infinite reservoir of reactants (the rest of the liquid volume), which maintains the reactant concentration constant during the reaction. Thus, one observed kinetics with an effective 0th order, hence the faster product formation. For further details on the origin of this effect, let us use the following notations

$$[InCl_3] = c(t) \tag{1}$$

$$[In(OH)_3] + [InCl_3] = c_0 \tag{2}$$

For the sake of simplicity, we assume a first-order reaction. In this case, the reaction rate r reads

$$r = \frac{d[In(OH)_3]}{dt} \tag{3}$$

$$= -\frac{d[InCl_3]}{dt} \tag{4}$$

$$= -\frac{dc(t)}{dt} = Kc(t) \tag{5}$$

where K is the rate constant of the reaction. This differential equation yields

$$[InCl_3] = c_0 e^{-Kt} \tag{6}$$

$$[In(OH)_3] = c_0(1 - e^{-Kt}) \tag{7}$$

$$r = c_0 K e^{-Kt} \tag{8}$$

Now, if the heated volume is much smaller than the size of the system, the concentration of $InCl_3$ can be considered as constant because $InCl_3$ molecules are continuously renewed in the heated region by Brownian motion. Equations 3 and 5 yield

$$r = \frac{d[In(OH)_3]}{dt} = Kc(t) \approx Kc_0 \tag{9}$$

and thus

$$[In(OH)_3] = Kc_0 t \tag{10}$$

The concentration of $In(OH)_3$ is thus linearly increasing as a function of time and no longer limited by an exponential saturation, as in eq 7. This mechanism is inherently related to the geometry of the system and can be seen as a natural Ostwald isolation.

DOI: 10.1021/acsomega.6b00019
ACS Omega 2016, 1, 2−8

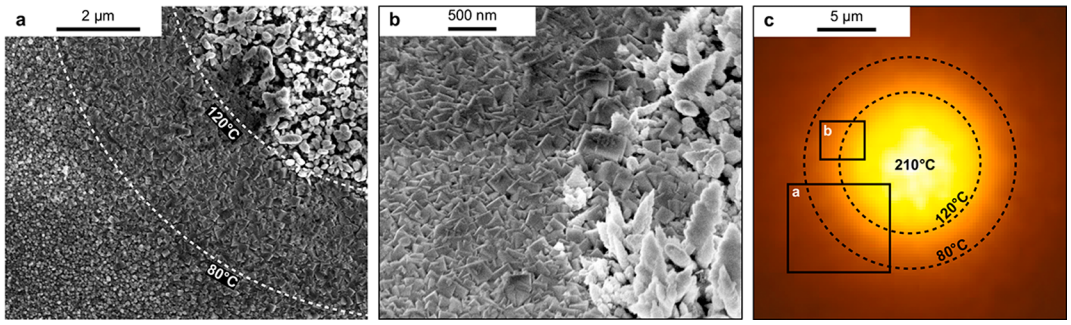

Figure 4. (a) SEM image of crystal formation along a temperature gradient. (b) SEM image highlighting the transition from one type of structure to another. The sample was imaged with a tilt angle of 45°. (c) Measured temperature distribution where the temperature thresholds (dashed lines) and the areas corresponding to the SEM images (a) and (b) (solid lines) have been indicated.

(3) The theory introduced above explains that the larger the system, the slower the reaction rate. It is certainly the reason why kinetics of crystal formation is so long with an autoclave, which usually implies heating duration longer than 20 h. A benefit of our approach is that we can observe the formation of crystals within only a few minutes, with the same reactant concentrations.

(4) Too long an exposure time (or too high a concentration) yields the formation of pine-tree-like structures, another type of structure (Figure 4b). Deviation from regular shapes for too long heating duration was also mentioned in the literature.[24] The reason was related to an Ostwald-ripening mechanism. If heating is carried further on or if we reproduce the exact same conditions of temperature, exposure time, and concentration as with an autoclave, one even observes the formation of a large and smooth dome (hemispherical structure) of the size of the heated area.

(5) It may seem surprising that the crystal products do not act as nucleation points for water boiling once they are formed, even at 200 °C. We have never observed bubble formation because of the formation of nano- and microcrystals. We believe that a nucleation center must consist of a microscale cavity (a scratch) rather than an asperity, a bump, to enable a flat initial curvature radius of a nucleating bubble, that is, a small Laplace overpressure. This is also the reason why the gold nanoparticles themselves do not act as nucleation points; they look like nanoscale bumps rather than microscale cavities.

(6) The heating dynamics can be as fast as the time scale $\tau = L^2/a$, where L is the characteristic size of the heated area and a is the thermal diffusivity of the surrounding medium. For water, $a = 10^{-7}$ $m^2 \cdot s^{-1}$. To give an idea, if the size of the heated area is $L = 10$ μm, the heating time scale can be as fast as 1 ms.

(7) Locally heating a fluid possibly yields fluid convection, even at the micrometric scale and especially when superheating a fluid. If the heated area is less than a micrometer, no strong convection is expected (less than a micrometer per second).[20] However, for a larger heated area, up to 100 μm, substantial convection can be observed (several 10 s of $\mu m \cdot s^{-1}$) and one can wonder what the effect could be on the chemical reaction. Our results show that convection does not affect the crystal growth. It should even favor kinetics by faster renewal of the reactants in the heated region. Furthermore, fluid convection is not supposed to affect the spatial steady-state distribution of temperature because temperature diffusion always occurs faster than thermal-induced fluid convection. This well-known effect in fluid dynamics stems from a large Prandtl number of water ($Pr \approx 7$).[25]

(8) Products remain located at the water/glass interface, where the nanoparticles are located. This may be because, in part, of the fact that it is where the temperature is the largest. However, the surface could also nucleate the formation of crystals by a heterogeneous nucleation process.

Effect of the Temperature Increase. A benefit of using our approach is that any dependence on the temperature increase can be easily studied. One can generate a temperature gradient on a single field-of-view, spanning from 200 °C to ambient temperature, and observe the morphological evolution of the formed crystals along the temperature gradient. Figure 4 presents such a situation. The temperature gradient was measured using our thermal microscopy technique and is displayed in Figure 4c. The resulting crystal formation was imaged using SEM, as presented in Figure 4a,b. We chose a situation where three different domains have been formed. The center domain, where the temperature was close to 200 °C, features the pine-tree-like structures observed when the heating duration is long enough (as mentioned earlier). The intermediate area, ranging from 120 to 80 °C, is covered with the cubic $In(OH)_3$ crystals of interest. Finally, the third zone is not covered with anything crystalline. Interestingly, the transition from one zone to another is extremely well defined and occurs at a precise temperature for a given heating duration. For instance, in the present case (i.e., for a heating duration of 1 h), the transition from pine-tree to cubic shapes occurs at $T = 120$ °C, and cubic crystals do not form below $T = 80$ °C. We used a long exposure time on purpose, to observe three domains. A shorter exposure time would have led to cubic crystals in the center of the heated area and to no pine-tree-like structures.

Noteworthily, in this experiment, one can see that the formation of crystals can be achieved at much lower temperatures than those expected (80−120 °C compared with 200 °C). This observation highlights an additional interest on PASC; because of enhanced kinetics, products can be obtained at reduced temperatures within a reasonable time, even under nonhydrothermal conditions.

DOI: 10.1021/acsomega.6b00019
ACS Omega 2016, 1, 2−8

DISCUSSION

Let us discuss the benefits of plasmon-assisted solvothermal chemistry (PASC) compared with those of using an autoclave at high pressure. (1) PASC yields much faster reactions, as explained above, because of an effective reduction of the order of the reaction by a natural Ostwald flooding. (2) PASC can achieve much faster heating/cooling dynamics, down to the microsecond scale. The temperature quasi-instantaneously rises or drops as soon as the laser illumination is turned on or off because of the weak inertia related to the small volume of the system. (3) PASC enables the observation of product formation using optical means, in real time (with a diffraction-limited resolution, not shown herein). (4) PASC enables the introduction of reactants during the reaction as the reaction medium is not sealed. (5) PASC makes the study of the effect of the temperature increase straightforward. A single experiment reveals the crystal morphologies over a full range of temperatures. (6) An industrial application could be the laser-driven microscale patterning of nano- and microcrystals, using a scanning laser.

It is also worth discussing the benefits of using a layer of gold nanoparticles (as the one displayed in Figure 1a), compared with those of using a uniform absorbing layer (like a metal layer for instance).[26] The real interest does not rely on the fact that plasmonic nanoparticles are much more absorbent. A substrate can be made nearly 100% absorbent without requiring plasmonic nanoparticles, and nanoparticles will never do better than 100% absorption. Also, even if the absorption is not large, the laser power can still be increased to reach the desired temperature. The benefits of using nanoparticles are the following. (1) The heated area can be much smaller than the size of a focused laser beam, down to the size of a single nanoparticle. (2) Metal films are highly reflective. With metal nanoparticles, it is possible to make the light−sample interaction purely absorbent (no scattering, no reflection, only absorption). (3) Depositing a metal layer requires bulky and expensive apparatus, whereas metal nanoparticle substrates (such as BCML samples) can be obtained using chemical means and cheap bench-top devices. (4) Plasmonic nanoparticles exhibit an absorption resonance in a finite region of the spectrum, which makes it possible to heat the sample at a given wavelength range, whereas the sample will remain transparent at other wavelengths. This will make, for instance, observation easier using optical microscopy techniques in the visible range upon heating in the IR range.

Let us now discuss the limitations of our technique. (1) It is not meant to produce large amounts of products (for industrial or commercial purposes for instance). It is rather intended to help fundamental research on solvothermal synthesis or to yield applications in local patterning of microstructures. (2) It is mainly of interest for solid-state products. If the products remain as dissolved species, the interest of PASC is not evident as the products will escape from the heated area because of Brownian motion. However, the production of solid products remains a major aspect of solvothermal synthesis, with a myriad of applications, from the synthesis of microporous crystals, ionic conductors, complex oxides and fluorides, low-dimensional aluminophosphates, inorganic−organic hybrid materials, and particularly condensed materials such as diamond and inorganic helical chains.[14]

Let us finally place the concept of PASC in the context of the state-of-the-art related to light-induced chemistry at the micrometric scale.

The concept of photothermal-induced growth of nano- and microstructures on plasmonic nanoparticles was pioneered by Boyd and coworkers in 2006[27] and then further investigated by other groups.[28−30] The concept introduced by Boyd consisted of a new chemical vapor deposition (CVD) process in which local heating necessary to induce the chemical deposition from a gas phase was performed by local laser heating at the micrometric scale of gold nanoparticles deposited on a substrate. The authors named this technique PACVD (plasmon-assisted CVD). They demonstrated microscale patterning of metal oxides such as PbO and TiO_2 on a glass substrate by local heating up to 150 °C. Their approach was, however, based on a gas environment, not involving a liquid environment in a superheated state, like in our study.

In 2009, Adleman and coworkers introduced the concept of plasmon-assisted catalysis (PAC) in a liquid environment. The authors chose to investigate the thermal-induced reforming of a liquid mixture of ethanol and water, leading to the formation of CO_2, CO, and H_2, favored by the natural catalytic effect of gold nanoparticles.[31,32] The experiments were conducted in a microfluidic channel to ease the collection of the gas products. However, no fluid superheating was involved in the mechanism.

In 2013, Yeo and coworkers[26] reported on the photothermal-induced growth of ZnO nanowires on a metal film acting as a light-absorbing layer. This seminal article is closely related to our work as the authors managed to grow microcrystals at the microscale using a photo-hydrothermal effect. However, the authors did not experimentally evidence fluid superheating (no temperature was measured), and they did not benefit from the plasmonic resonance of metal nanoparticles.

In 2015, Kwon and coworkers[33] reported on the photothermal-induced formation of metal-oxide (CuO and ZnO) structures in aqueous precursor solution. Here, again the temperature was not monitored and the authors did not benefit from the use of plasmonic nanoparticles. Moreover, the authors did not manage to produce crystalline structures, presumably because of the aforementioned issue, which occurs when the reactant concentration is too high or the heating duration is too long.

CONCLUSIONS

In summary, we report on an experimental technique suited to conduct solvothermal synthesis at ambient pressure, on a small scale, using plasmonic nanoparticles acting as light absorbers and nanosources of heat. We illustrate the principle with the synthesis of $In(OH)_3$ microcrystals at 200 °C in liquid water. To evidence the similarities and the differences compared with common high-pressure experiments, the effects of several parameters have been investigated: the reactant concentration, the magnitude of the temperature increase, the heating duration, and the size of the heated area. Several singular effects have been evidenced. (1) The smaller the heated region, the faster the reaction, because of an Ostwald flooding effect. Although an autoclave approach usually implies heating times longer than 20 h, one can achieve crystal formation within a few minutes using PASC. (2) A long enough heating duration leads to another type of structure (pine trees). (3) Reproducing the exact same conditions of temperature, concentration, and duration as with an autoclave approach does not lead to the formation of microcrystals. Because of too fast kinetics, we

DOI: 10.1021/acsomega.6b00019
ACS Omega 2016, 1, 2−8

rather observe the formation of a large, smooth dome. (4) The temperature dependence on the crystal morphology can be investigated in a one-shot experiment by creating a microscale temperature gradient. (5) Solvothermal reactions that normally occur in a superheated fluid can be achieved at much lower temperatures within a reasonable amount of time because of much faster kinetics. (6) Microcrystal products do not act as nucleation points for bubble formation and do not prevent the fluid from superheating. (7) Microcrystal products remain located at the substrate/solvent interface and do not diffuse in the surrounding solvent. (8) The presence of thermal-induced microscale fluid convection does not affect the crystal growth.

This work gives the guidelines for efficient solvothermal chemistry at the microscale at ambient pressure and could pave the way for new approaches suited for fundamental research on solvothermal synthesis or for practical applications in microscale patterning of nanostructures. More sophisticated PASC approaches could further benefit from the natural catalytic effect of gold nanoparticles.

AUTHOR INFORMATION

Corresponding Authors

*E-mail: hadrien.robert@fresnel.fr (H.R.).
*E-mail: guillaume.baffou@fresnel.fr (G.B.).

Notes

The authors declare the following competing financial interest(s): HR has been a PhD student from April 2015 with financial support that came partly from the Phasics SA company.

ACKNOWLEDGMENTS

This work was partly supported by the Agence Nationale de la Recherche (Grant NATO, ANR-13-BS10-0013-03). J.P. and F.K. thank Prof. R. Fässler and the Max Plank society, which financially supported this work. R.Q. and E.B.-U. acknowledge financial support from the European Community's Seventh Framework Program under grant ERC-Plasmolight (259196), the Spanish Ministry of Economy and Competitiveness, through the 'Severo Ochoa' Programme for Centres of Excellence in R&D (SEV-2015-0522) and Fundació CELLEX Barcelona. E.B.-U. acknowledges the support of the FPI fellowship from the Spanish Ministry of Science and Innovation (MICINN).

REFERENCES

(1) Baffou, G.; Quidant, R. Nanoplasmonics for Chemistry. *Chem. Soc. Rev.* **2014**, *43*, 3898−3907.

(2) Kale, M. J.; Avanesian, T.; Christopher, P. Direct Photocatalysis by Plasmonic Nanostructures. *ACS Catal.* **2014**, *4*, 116−128.

(3) Zhang, X.; Chen, Y. L.; Liu, R. S.; Tsai, D. P. Plasmonic Photocatalysis. *Rep. Prog. Phys.* **2013**, *76*, 046401.

(4) Wang, C.; Astruc, D. Nanogold plasmonic photocatalysis for organic synthesis and clean energy conversion. *Chem. Soc. Rev.* **2014**, *43*, 7188.

(5) Qiu, J.; Wei, W. D. Surface Plasmon-Mediated Photothermal Chemistry. *J. Phys. Chem. C* **2014**, *118*, 20735−20749.

(6) Adleman, J. R.; Boyd, D. A.; Goodwin, D. G.; Psaltis, D. Heterogenous Catalysis Mediated by Plasmon Heating. *Nano Lett.* **2009**, *9*, 4417−4423.

(7) Fasciani, C.; Alejo, C. J. B.; Grenier, M.; Netto-Ferreira, J. C.; Scaiano, J. C. High-Temperature Organic Reactions at Room Temperature Using Plasmon Excitation: Decomposition of Dicumyl Peroxide. *Org. Lett.* **2011**, *2*, 204−207.

(8) Vásquez-Vásquez, C.; Vaz, B.; Giannini, V.; Pérez-Lorenzo, M.; Alvarez-Puebla, R. A.; Correa-Duarte, M. A. Nanoreactors for Simultaneous Remote Thermal Activation and Optical Monitoring of Chemical Reactions. *J. Am. Chem. Soc.* **2013**, *135*, 13616−13619.

(9) Yen, C. W.; El-Sayed, M. A. Plasmonic Field Effect on the Hexacyanoferrate(III)-Thiosulfate Electron Transfer Catalytic Reaction on Gold Nanoparticles: Electromagnetic or Thermal? *J. Phys. Chem. C* **2009**, *113*, 19585−19590.

(10) Hung, W. H.; Aykol, M.; Valley, D.; Hou, W.; Cronin, S. B. Plasmon Resonant Enhancement of Carbon Monoxide Catalysis. *Nano Lett.* **2010**, *10*, 1314−1318.

(11) Lee, J.; Mubeen, S.; Li, X.; Stucky, G. D.; Moskovits, M. Plasmonic Photoanodes for Solar Water Splitting with Visible Light. *Nano Lett.* **2012**, *12*, 5014−5019.

(12) Warren, S. C.; Thimsen, E. Plasmonic Solar Water Splitting. *Energy Environ. Sci.* **2012**, *5*, 5133.

(13) Brongersma, M. L.; Halas, N. J.; Nordlander, P. Plasmon-Induced Hot Carrier Science and Technology. *Nat. Nanotechnol.* **2015**, *10*, 25−34.

(14) Feng, S.; Xu, R. New Materials in Hydrothermal Synthesis. *Acc. Chem. Res.* **2001**, *34*, 239−247.

(15) Baffou, G.; Polleux, J.; Rigneault, H.; Monneret, S. Super-Heating and Micro-Bubble Generation around Plasmonic Nanoparticles under cw Illumination. *J. Phys. Chem. C* **2014**, *118*, 4890.

(16) Baffou, G.; Quidant, R. Thermo-Plasmonics: Using Metallic Nanostructures as Nano-Sources of Heat. *Laser Photonics Rev.* **2013**, *7*, 171−187.

(17) Kundrat, F.; Baffou, G.; Polleux, J. Shaping and Patterning Gold Nanoparticles via Micelle Templated Photochemistry. *Nanoscale* **2015**, *7*, 15814−15821.

(18) Baffou, G.; Bon, P.; Savatier, J.; Polleux, J.; Zhu, M.; Merlin, M.; Rigneault, H.; Monneret, S. Thermal Imaging of Nanostructures by Quantitative Optical Phase Analysis. *ACS Nano* **2012**, *6*, 2452−2458.

(19) Zhu, H.; Yao, K.; Wo, Y.; Wang, N.; Wang, L. Hydrothermal synthesis of single crystalline $In(OH)_3$ nanorods and their characterization. *Semicond. Sci. Technol.* **2004**, *19*, 1020−1023.

(20) Donner, J.; Baffou, G.; McCloskey, D.; Quidant, R. Plasmon-Assisted Optofluidics. *ACS Nano* **2011**, *5*, 5457−5462.

(21) Würger, A. Thermal Non-Equilibrium Transport in Colloids. *Rep. Prog. Phys.* **2010**, *73*, 126601.

(22) Iacopini, S.; Piazza, R. Thermophoresis in Protein Solutions. *Europhys. Lett.* **2003**, *63*, 247−253.

(23) Duhr, S.; Braun, D. Why Molecules Move along a Temperature Gradient. *Proc. Natl. Acad. Sci. U.S.A.* **2006**, *103*, 19678.

(24) Tang, S.; Zhang, J.; Wu, S.; Hu, C.; Li, Y.; Jiang, L.; Cui, Q. Effects of Heating Rate on the Nucleation, Growth, and Transformation of InOOH and In_2O_3 via Solvothermal Reactions. *J. Phys. Chem. C* **2014**, *118*, 21170−21176.

(25) Guyon, E.; Hulin, J. P.; Petit, L.; Mitescu, C. D. *Physical Hydrodynamics*; Oxford University Press: USA, 2001.

(26) Yeo, J.; Hong, S.; Wanit, M.; Kang, H. W.; Lee, D.; Grigoropoulos, C. P.; Sung, H. J.; Ko, S. H. Rapid, One-Step, Digital Selective Growth of ZnO Nanowires on 3D Structures Using Laser Induced Hydrothermal Growth. *Adv. Funct. Mater.* **2013**, *23*, 3316−3323.

(27) Boyd, D. A.; Greengard, L.; Brongersma, M.; El-Naggar, M. Y.; Goodwin, D. G. Plasmon-Assisted Chemical Vapor Deposition. *Nano Lett.* **2006**, *6*, 2592−2597.

(28) Cao, L.; Barsic, D. N.; Guichard, A. R.; Brongersma, M. L. Plasmon-Assisted Local Temperature Control to Pattern Individual Semiconductor Nanowires and Carbon Nanotubes. *Nano Lett.* **2007**, *7*, 3523−3527.

(29) Hwang, D. J.; Ryu, S. G.; Grigoropoulos, C. P. Multi-Parametric Growth of Silicon Nanowires in a Single Platform by Laser-Induced Localized Heat Sources. *Nanotechnology* **2011**, *22*, 385303.

(30) Hung, W. H.; Hsu, I. K.; Bushmaker, A.; Kumar, R.; Theiss, J.; Cronin, S. B. Laser Directed Growth of Carbon-Based Nanostructures by Plasmon Resonant Chemical Vapor Deposition. *Nano Lett.* **2008**, *8*, 3278−3282.

DOI: 10.1021/acsomega.6b00019
ACS Omega 2016, 1, 2−8

(31) Haruta, M.; Kobayashi, T.; Sano, H.; Yamada, N. Novel Gold Catalysts for the Oxidation of Carbon Monoxide at a Temperature Far below 0 °C. *Chem. Lett.* **1987**, *16*, 405−408.
(32) Cho, A. Connecting the Dots to Custom Catalysts. *Science* **2003**, *299*, 1684−1685.
(33) Kwon, K.; Shim, J.; Lee, J. O.; Choi, K.; Yu, K. Localized Laser-Based Photohydrothermal Synthesis of Functionalized Metal-Oxides. *Adv. Funct. Mater.* **2015**, *25*, 2222−2229.

DOI: 10.1021/acsomega.6b00019
ACS Omega 2016, 1, 2−8